energy&fuels

pubs.acs.org/EF

Article

# Combustion of $n$-$C_3$−$C_6$ Linear Alcohols: An Experimental and Kinetic Modeling Study. Part II: Speciation Measurements in a Jet-Stirred Reactor, Ignition Delay Time Measurements in a Rapid Compression Machine, Model Validation, and Kinetic Analysis

M. Pelucchi,* S. Namysl, E. Ranzi, A. Rodriguez, C. Rizzo, K. P. Somers, Y. Zhang, O. Herbinet, H. J. Curran, F. Battin-Leclerc, and T. Faravelli

Cite This: *Energy Fuels* 2020, 34, 14708−14725

Read Online

ACCESS | Metrics & More | Article Recommendations | Supporting Information

**ABSTRACT:** This work presents new experimental data for $n$-$C_3$−$C_6$ alcohol, combustion ($n$-propanol, $n$-butanol, $n$-pentanol, $n$-hexanol). Speciation measurements have been carried out in a jet-stirred reactor ($p$ = 107 kPa, $T$ = 550−1100 K, $\varphi$ = 0.5, 1.0, 2.0) for $n$-butanol, $n$-pentanol, and $n$-hexanol. Ignition delay times of ethanol, $n$-propanol, $n$-butanol, and $n$-pentanol/air mixtures were measured in a rapid compression machine at $\varphi$ = 1.0, $p$ = 10 and 30 bar, and $T$ = 704−935 K. The kinetic subsets for alcohol pyrolysis and oxidation from the CRECK kinetic model have been systematically updated to describe the pyrolysis and high- and low-temperature oxidation of this series of fuels as described in Part I of this work (Pelucchi, M.; Namysl, S.; Ranzi, E. et al. Combustion of $n$-C3−C6 linear alcohol: an experimental and kinetic modeling study. Part I: reaction classes, rate rules, model lumping and validation. Submitted to Energy and Fuels, 2020). Part II describes in detail the facilities used for this systematic experimental investigation of $n$-$C_3$−$C_6$ alcohol combustion and presents a complete validation of the kinetic model by means of comparisons with the new data and measurements previously reported in the literature for both pyrolytic and oxidative conditions. Kinetic analyses such as rate of production and sensitivity analyses are used to highlight the governing reaction pathways and reasons for existing deviations, motivating possible further improvements in our chemistry mechanism.

## 1. INTRODUCTION

As highlighted in Part I,[1] alcohol are promising alternative fuels, as well as blending fuel components for internal combustion engines.[2,3] Alcohols thus constitute a valuable and viable solution to the negative impact of the transport sector on the environment and on human health. The development of detailed and predictive combustion kinetic models provides a very efficient tool for the synergistic design of fuels and engines,[4] thus guiding the implementation of alternative routes for energy production and utilization. This work completes Part I[1] by describing in detail the experimental facilities and methods used for a systematic investigation of linear $n$-$C_3$−$C_6$ alcohols. New ignition delay time (IDT) data for ethanol, $n$-propanol, $n$-butanol, and $n$-pentanol have been measured in a rapid compression machine (RCM). Speciation data for $n$-butanol, $n$-pentanol, and $n$-hexanol have been acquired in a jet-stirred reactor (JSR), allowing detailed insights into intermediate species formed during their oxidation. The brief preliminary validation reported in Part I is extended here to a larger number of experimental targets covering pyrolysis and oxidation over a wide range of temperatures, pressures, and dilution conditions. The validation of the model is supported by a detailed kinetic analysis and a thorough discussion on the governing pathways in the pyrolysis and oxidation of alcohols. A further demonstration of the validity of the approach and of the rate rules adopted is obtained by extending the same rate rules to describe $n$-octanol oxidation. Due to space limitations, the most important aspects of the model validation are described in detail herein, with factors of secondary and minor importance described in detail in the Supporting Information. The article is organized as follows: Section 2 presents the experimental methodology adopted for the RCM measurements (Section 2.1) and for the JSR measurements (Section 2.2). The model presented in Part I[1] is validated in Section 3 by comparing its predictions to different experimental targets. The validation hierarchically covers pyrolysis and high- and low-temperature oxidation, thus providing a comprehensively validated kinetic model for $n$-$C_3$−$C_6$ alcohol combustion.

## 2. EXPERIMENTAL METHODS

This section describes the experimental facilities used to investigate the oxidation of linear alcohols at low to intermediate temperatures, using an RCM and a JSR. Table 1 summarizes the operating conditions of the experimental measurements carried out in this study for the different fuels. 2.1Sections 2.1 and 2.2 describe the experimental apparatuses in detail.

**Received:** July 7, 2020
**Revised:** October 14, 2020
**Published:** October 27, 2020

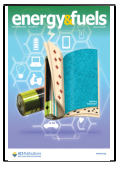

**Table 1. Operating Conditions of the Experimental Measurements in JSR and RCM Carried Out in This Study[a]**

| Jet-Stirred Reactor | | | | |
|---|---|---|---|---|
| fuel (0.5−$O_2$/He) | $\varphi$ | temperature [K] | pressure [bar] | $\tau$ [s] |
| *n*-butanol | 0.5, 1.0, 2.0 | 500−1100 | 1.07 | 2.0 |
| *n*-pentanol | 0.5, 1.0, 2.0 | 500−1100 | 1.07 | 2.0 |
| *n*-hexanol | 0.5, 1.0, 2.0 | 500−1100 | 1.07 | 2.0 |
| Rapid Compression Machine | | | | |
| fuel in "air" | $\varphi$ | temperature [K] | pressure [bar] | dilution |
| ethanol | 1.0 | 893−926 | 10.0 | 50% $N_2$, 50% Ar |
| | 1.0 | 826−909 | 30.0 | 40% $N_2$, 60% Ar |
| *n*-propanol | 1.0 | 877−935 | 10.0 | 50% $N_2$, 50% Ar |
| | 1.0 | 800−900 | 30.0 | 50% $N_2$, 50% Ar |
| *n*-butanol | 1.0 | 824−924 | 10.0 | 30% $N_2$, 70% Ar |
| | 1.0 | 727−844 | 30.0 | 90% $N_2$, 10% Ar |
| | 1.0 | 704−735 | 30.0 | 70% $N_2$, 30% $CO_2$ |
| *n*-pentanol | 1.0 | 710−833 | 10.0 | 100% $N_2$ |
| | 1.0 | 813−926 | 10.0 | 50% $N_2$, 50% Ar |

[a]Compositions are in molar units.

**2.1. Ignition Delay Time Measurements in NUI Galway RCM: Ethanol, *n*-Propanol, *n*-Butanol, and *n*-Pentanol.** Low-to-intermediate-temperature IDTs for stoichiometric fuel/air mixtures of four alcohols including ethanol, *n*-propanol, *n*-butanol, and *n*-pentanol were measured in an RCM at NUI Galway at conditions relevant to those encountered in internal combustion engines, at $p$ = 10−30 bar and $T$ = 704−935 K. All mixtures were prepared manometrically in two stainless steel tanks preheated to 80 °C. The tanks were evacuated to $10^{-3}$ bar prior to mixture preparation. The required volume of fuel was first injected into the tanks by a calibrated syringe, and the pressure was monitored so that the appropriate partial pressure of fuel (i.e., one-third of the vapor pressure at 80 °C to avoid condensation) was present in the mixing vessels. All intake manifolds connected to the RCM were also heated to 80 °C. The fuels, ethanol (>99.5%), propanol (99%), *n*-butanol (99%), and *n*-pentanol (99%), were obtained from Sigma-Aldrich. $O_2$, $N_2$, Ar and $CO_2$ were supplied by BOC Ireland and Air Liquide at 99.5, 99.95, 99.9995, and 99.5%, respectively.

The RCM is a horizontally opposed twin-piston device that has been described previously.[5,6] Briefly, the symmetry of the RCM allows for a short adiabatic compression time (16−17 ms) and helps in creating and maintaining a high-temperature and -pressure environment while minimizing heat loss effects inside the combustion chamber during compression.[7] The pistons are locked at the stroke-end, thus allowing a near-constant volume reaction to proceed. The piston head features large crevices to remove the formation of in-cylinder roll-up vortices within the boundary layer gases. This design helps the mixture and the temperature in the reaction chamber to be near-homogeneous prior to ignition. The compressed temperatures and pressures before the main ignition event are reached by changing the initial pressures and temperatures, starting from 30 °C to ensure that the fuel was fully vaporized. For each temperature, we performed five ignition experiments, to ensure repeatability. For all of the experiments, the positions of both pistons are recorded using a digital oscilloscope, while the pressure profiles were recorded using a pressure transducer (Kistler 603B). Piston positioning is monitored using a Positek P100 linear inductive position sensor, which is inserted into the RCM's hollow connecting rod. Both the pressure and piston position traces are recorded using a PicoScope 4424 digital oscilloscope. The IDT is defined as the time difference between the peak in pressure at the end of the compression and the maximum rate of pressure rise due to fuel reactivity/ignition. The temperatures are calculated using GasEq,[8] considering the mixture composition and initial temperature, initial pressure, and compressed gas pressure under the assumption of adiabatic compression and frozen chemistry. For each experimental condition, a nonreactive experiment is performed, by replacing oxygen with nitrogen in the test mixture, to ensure comparable thermodynamic properties to determine the facility effects needed in the numerical simulations. The experimental uncertainty is estimated to be 2% in the reported temperature and 25% in reported IDTs, due mainly to the uncertainties in the initial temperature (±3−13 K).[9] Ignition data and volume profiles for each tested condition are reported in the Supporting Information.

**2.2. Speciation Measurements in CNRS Nancy JSR: *n*-Butanol, *n*-Pentanol, and *n*-Hexanol.** The JSR used here has been often used for kinetic studies of pyrolysis and combustion.[10,11] Moreover, by analogy with the results presented in this study for *n*-$C_4$−$C_6$ alcohols, recently, the oxidation of *n*-$C_4$−$C_6$ aldehydes[12] and of *n*-$C_4$−$C_5$ organic acids (butanoic and pentanoic) has been investigated.[13] This study also aims at complementing these previous studies.

The JSR at Nancy consists of a fused silica sphere (volume of 92 $cm^3$) equipped with four injection nozzles positioned at right angles to one another at the center of the sphere. This injection method ensures high turbulences in the reactor and leads to homogeneity in both temperature and product concentration of the gas phase. The isothermal JSR is preceded by a quartz annular preheat zone, in which the temperature of the gas is increased to the reactor temperature. The gas residence time inside the annular preheater is very short compared to its residence time inside the reactor (a few percent) to avoid any reactivity in this section. The heating is ensured by resistances (Thermocoax) rolled around the reactor and the preheat zone, which allows flexibility and swiftness in the heating of each area. Temperatures are measured using K-type thermocouples located inside the inlet cross and between the resistances and the external wall of the reactor. The reaction temperature is assumed to be equal to that measured in the inlet cross according to the isothermal reactor hypothesis, with a gradient of 5 K.

This study was performed between 500 and 1100 K at 107 kPa at three equivalence ratios ($\varphi$ = 0.5, 1.0, 2.0) for *n*-butanol, *n*-pentanol, and *n*-hexanol. Fuels were provided by Sigma-Aldrich with a purity of ≥99%. Helium (99.999%) and oxygen (99.999%) were provided by Messer. Gas flow rates were controlled by mass flow controllers and liquid flow rate by a Coriolis flow controller, followed by a vaporization chamber maintained at 10 K above each fuel boiling temperature. The uncertainty in the flow measurements was around 0.5% for each controller, so about 2% on the residence time.

The reactor outlet gas was transported by a heated line to GCs. The first chromatograph, equipped with a Carbosphere packed column and a thermal conductivity detector (TCD), was used for the quantification of light-weight compounds such as oxygen, methane, ethylene, acetylene, and ethane. The second chromatograph is fitted with a Q-Bond capillary column, and an FID preceded by a methanizer was used for the quantification of compounds containing from one carbon atom to compounds containing up to five carbon atoms. The methanizer (nickel catalyst for hydrogenation) made it possible to detect species such as CO, $CO_2$, and $CH_2O$ with a good sensitivity. A third chromatograph was equipped with an HP-5 capillary column and an FID for the detection of the heaviest compounds. The identification of reaction products was performed using a gas chromatograph equipped with both types of capillary columns and coupled to a quadrupole mass spectrometer. Calibrations were performed by injecting standards or using the effective carbon number method when standards were not available (FID only). The maximum relative error in mole fractions was estimated to be ±5% for the species calibrated with standards and ±10% for species calibrated using the effective carbon number method. It should be noted that, due to the low vapor pressure of the larger alcohols including *n*-pentanol and *n*-hexanol, the uncertainty in the mole fractions of these species is larger than the values typically obtained for hydrocarbons of similar molecular weight (≈5%). The relative uncertainty is estimated to be approximately 10%. Experimental data are reported in a tabular form in the Supporting Information.


https://dx.doi.org/10.1021/acs.energyfuels.0c02252
Energy Fuels 2020, 34, 14708−14725

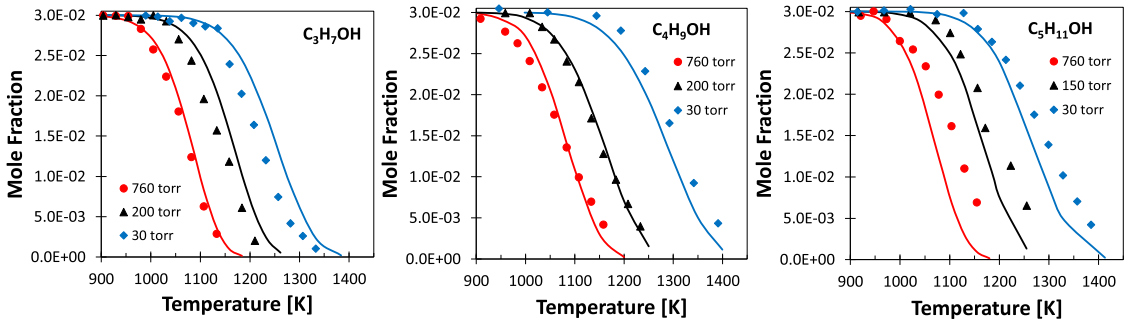


**Figure 1.** Experimental (symbols)[15−17] and simulated (solid lines) mole fraction profiles of *n*-propanol, *n*-butanol, and *n*-pentanol at $p$ = 30, 200, and 760 Torr.

## 3. RESULTS AND DISCUSSION

The kinetic model validated and discussed in the following sections has been described in detail in Part I[1] and is attached as the Supporting Information. Kinetic simulation, rate of production, and sensitivity analyses have been performed using the OpenSMOKE++ framework (Version 12.0) by Cuoci et al.[14]

**3.1. Pyrolysis.** *3.1.1. Pyrolysis of n-Propanol, n-Butanol, and n-Pentanol in a Hefei Flow Reactor.* The thermal decomposition of *n*-propanol, *n*-Butanol, and *n*-pentanol was studied in a flow reactor at the National Synchrotron Radiation Laboratory in Hefei, China.[15−17] Mixtures of 3% fuel in argon have been systematically tested at pressures between 30 and 760 Torr and temperatures $T$ = 800−1400 K in three different studies over the last few years. The species formed during pyrolysis were identified using molecular beam mass spectrometry. Methodologies adopted in Hefei for the identification through measurements of photoionization efficiency (PIE) are reported in the study by Cai et al.[15]

Figure 1 compares experimental fuel mole fraction profiles with model predictions at pressures of 30, 200, and 760 Torr. The measured temperature distributions along the flow tube centerline are used in the simulation. The model reproduces the temperature dependence quite accurately with maximum deviations always being within the experimental uncertainty (±30 K), with the exception of the highest-temperature branch of *n*-pentanol conversion.

A more detailed comparison of experimental and simulated mole fraction profiles of the three fuels, intermediate and product species, is reported in Figure 2 for the 760 Torr case. Additional comparisons at different pressures are reported in the Supporting Information material (Figures S1−S3). As expected from the longer chain length and similar reactor operating conditions, the different reactivity of the three fuels, if any, should follow the trend predicted by the model (i.e., pentanol > butanol > propanol). Similar trends have been obtained by testing the model of Sarathy et al.[18]

In general, good agreement is observed for *n*-propanol and *n*-butanol. However, propanal ($C_2H_5CHO$) formation is underestimated by a factor of ≈3 in the case of *n*-propanol. According to model predictions, propanal is mostly formed by the $\beta$-scission reaction of the $\alpha$ radical ($CH_3CH_2\dot{C}HOH = C_2H_5CHO + \dot{H}$) and by the four-centered molecular dehydrogenation reaction ($nC_3H_7OH = C_2H_5CHO + H_2$). The first one also indicates the appropriateness of the selected rate parameters for H-atom abstraction reactions and of the relative selectivity to the different H-atom abstraction sites. In this perspective, it should be noted that the same reaction classes (see Part I[1]) are responsible for the formation of butanal ($C_3H_7CHO$) for *n*-butanol pyrolysis, which, in that case, is overestimated by a factor of ≈2. Arguably, no evidence of *n*-pentanal was reported by Wang et al.[17] for *n*-pentanol pyrolysis. Aiming at defining a set of rate rules for reaction classes, these types of observations and inconsistencies were also used to guide the selection of the reference rate parameters described in Section 3. Good agreement in terms of selectivity to $C_n$ aldehyde formation is observed for the Ghent flow reactor cases presented in Figure 3.

In the case of *n*-butanol, some deviation is observed in the acetaldehyde ($CH_3CHO$) profiles. Acetaldehyde is mostly produced by the $\beta$-scission reaction of an $\alpha$ radical ($CH_3CH_2CH_2\dot{C}HOH = CH_3CHO + \dot{C}_2H_5$) where we assume that ethenol is directly transformed into $CH_3CHO$ through a tautomerization reaction. Most of the deviations observed for *n*-pentanol are explained by the excessive conversion of the fuel at $T$ > 1000 K. In terms of the relative amounts of intermediate species, the model overpredicts by a factor of 2 the peak in formaldehyde ($CH_2O$). Similar to *n*-propanol and *n*-butanol, formaldehyde is mostly formed by the fast $\beta$-scission of $R\dot{O}$ radicals ($R\dot{O} = CH_2O + \dot{C}_{n-1}$ alkyl radical) whose relative amount decreases with the increasing chain length. In addition, unimolecular $C_\beta-C_\alpha$ fissions produce hydroxyl-methyl radicals ($\dot{C}H_2OH$) that further decompose into formaldehyde and $\dot{H}$ atoms. The importance of this channel also decreases for the increasing molecular weight.

Based on the above observations of the relative importance of the pathways for the formation of formaldehyde and their dependence on the fuel molecule carbon chain length, one would expect the order *n*-propanol> *n*-butanol> *n*-pentanol. From the experimental data, the trend is instead *n*-butanol > *n*-propanol > *n*-pentanol. The inversion between *n*-propanol and *n*-butanol is explained by the $\beta$-scission reaction of the additional secondary radical available for *n*-butanol, producing $\dot{C}H_2OH$ ($CH_3\dot{C}HCH_2CH_2OH = C_3H_6 + \dot{C}H_2OH$). Pentene is formed through the four-centered molecular dehydration of *n*-pentanol and by the $\beta$-scission reaction of $\beta$-radicals, producing OH and a $C_n$ alkene. Again, a twofold overestimation is observed.

*3.1.2. Pyrolysis of n-Butanol and n-Pentanol in a Ghent Flow Reactor.* *n*-Butanol and *n*-pentanol pyrolysis (50% fuel/nitrogen) was also investigated in the flow reactor of the bench-scale setup at Ghent University,[19,20] at $T$ = 630−850 °C and $p$ = 1.7 bar. Gas samples were injected online on a GC equipped with an FID to quantify $C_4$ species. Small oxygenated species such as formaldehyde, methanol, and water were identified in an additional chromatograph. Permanent gases were quantified with two thermal conductivity detectors (TCDs). An online GC × GC was used to identify and quantify the species, using a


https://dx.doi.org/10.1021/acs.energyfuels.0c02252
Energy Fuels 2020, 34, 14708−14725

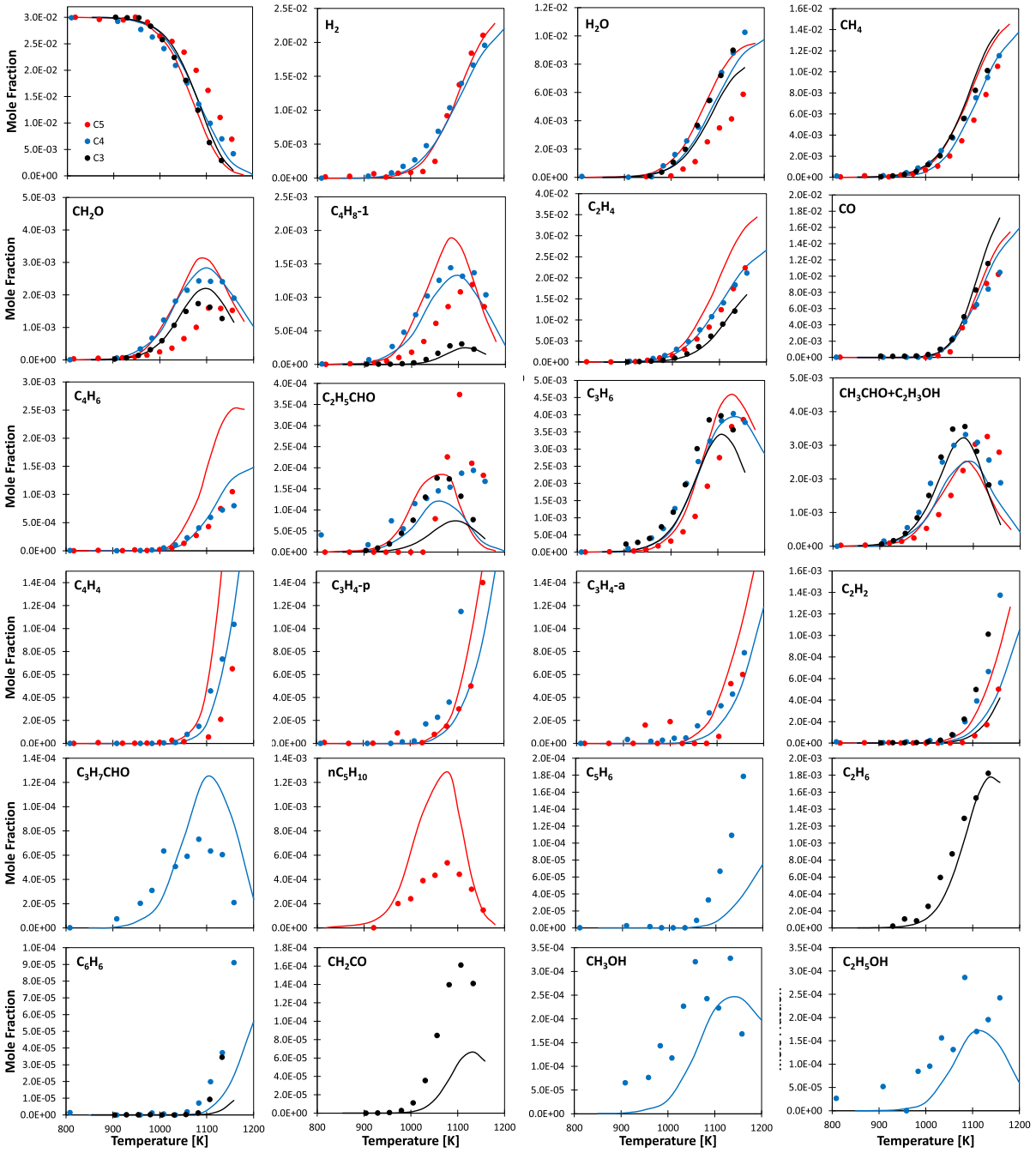


**Figure 2.** Experimental (symbols)[15−17] and simulated (solid lines) mole fraction profiles of reactants and products quantified during the pyrolysis of n-propanol, n-butanol, and n-pentanol at $p$ = 760 Torr. Composition: 3% fuel, 97% Ar.

time-of-flight mass spectrometer (TOF−MS) and a flame ionization detector, respectively.

Fuel conversion and intermediate species profiles are reported in Figure 3. The measured process gas temperature profiles are used in the simulations. The model predicts the fuel conversion profiles within experimental uncertainty and the expected trend in the decomposition rate of *n*-pentanol> *n*-butanol. Moreover, contrary to the comparisons with the data from the Hefei flow reactor, the conversion of *n*-pentanol is correctly predicted. Yields of acetaldehyde that were overestimated in Figure 2 are here underestimated by the same amount, supporting the selection of rate constants for the reaction classes responsible for $CH_3CHO$ formation discussed in Part I.[1] The formation of $C_n$ alkenes confirms the overestimation of pentene from *n*-pentanol, while good agreement is observed for $C_4H_8$-1 (1-butene). Analogous reaction pathways lead to the formation of the corresponding 1-alkene for the two fuels: the $\beta$-scission reactions of the lumped $\dot{R}_{(B)}$ radical in *n*-pentanol and $\beta$-radical in *n*-butanol and, to a lesser extent, from the dehydration reaction. Formaldehyde is slightly underpredicted for both fuels, counterbalancing the modest performances observed in Figure 2 for *n*-pentanol.

Both in the Ghent (Figure 3) and Hefei (Figure 2) flow reactors, the formation of butadiene ($C_4H_6$) from *n*-pentanol is overpredicted. $C_4H_6$ comes from successive reactions (i.e., H-abstraction reactions and radical decompositions) of 1-pentene ($nC_5H_{10}$), producing resonantly stabilized pentenyl radicals ($nC_5\dot{H}_9$-3 in the kinetic model nomenclature) that decompose


https://dx.doi.org/10.1021/acs.energyfuels.0c02252
*Energy Fuels* 2020, 34, 14708−14725

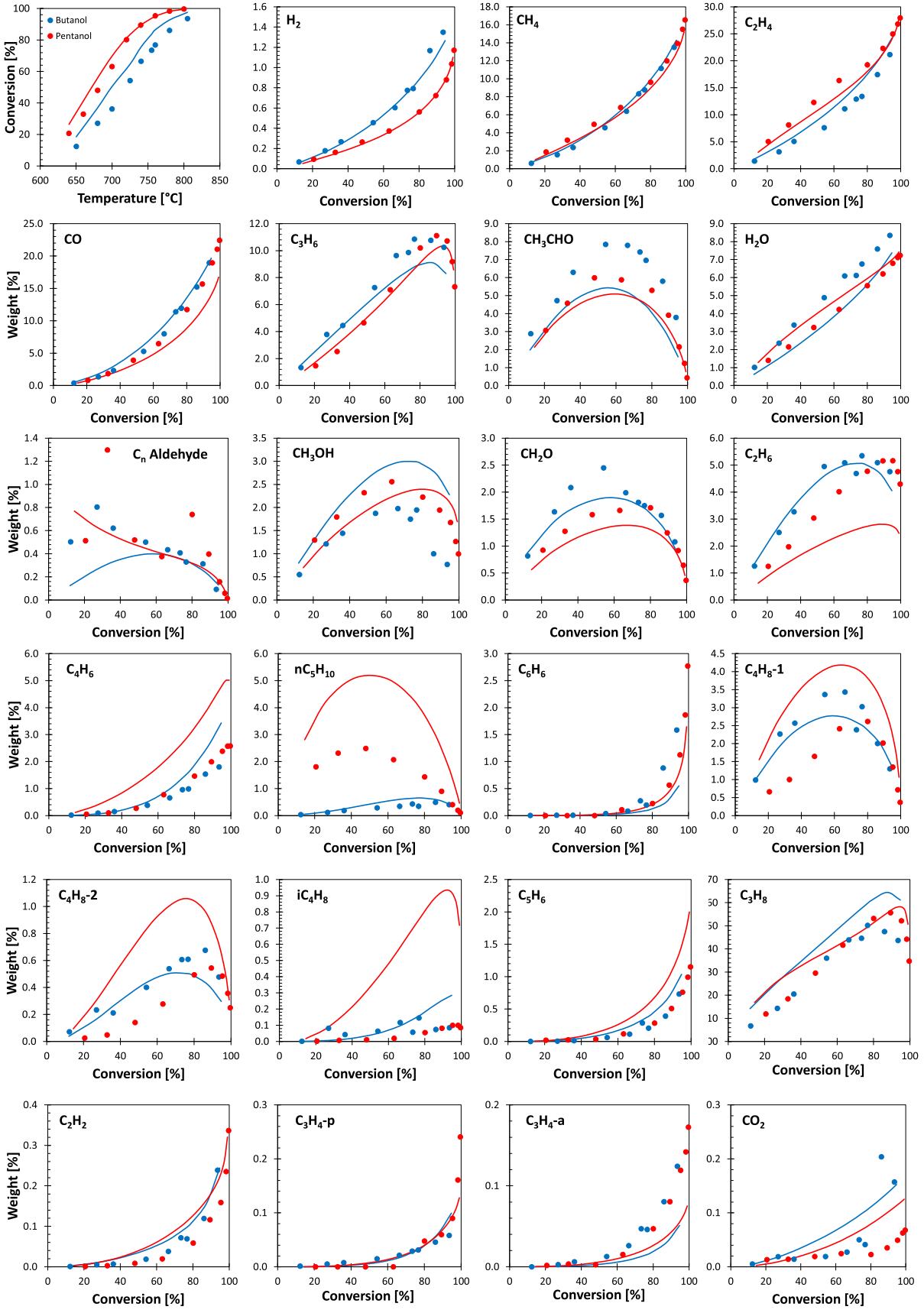


**Figure 3.** Experimental data (symbols)[19,20] and simulations (lines) for *n*-butanol and *n*-pentanol pyrolysis (50% fuel in $N_2$) at $T = 630–850$ °C, $p = 1.7$ bar. The top-left panel shows fuel conversion as a function of reactor temperature, while other panels show the mass fraction of intermediate and product species as function of fuel conversion.



https://dx.doi.org/10.1021/acs.energyfuels.0c02252
*Energy Fuels* 2020, 34, 14708−14725

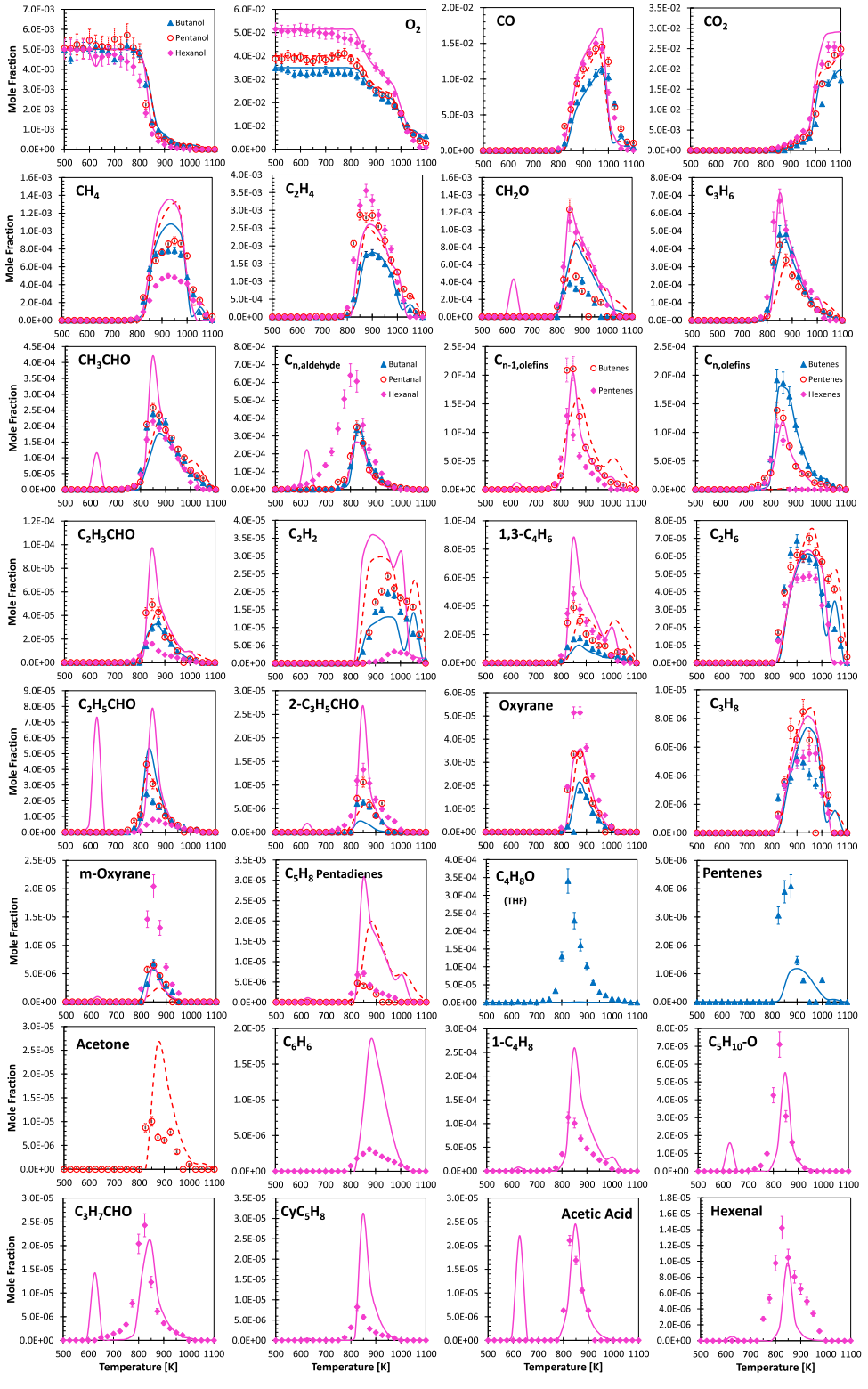


**Figure 4.** *n*-butanol, *n*-pentanol, and *n*-hexanol oxidation in JSR at $\varphi = 1.0$, $p = 107$ kPa, and $\tau = 2.0$ s. Comparison between experimental (symbols) and predicted (lines) mole fraction profiles of intermediate and product species.

into butadiene and methyl radicals. 1-pentene, whose peak concentration is also overpredicted in both cases, is mostly produced from the $\beta$-scission reactions of the lumped ($\dot{B}$) radical.

Despite its minor quantities (<1% of fuel conversion), *iso*-butene ($iC_4H_8$) is well predicted in the case of *n*-butanol and largely overpredicted in the case of *n*-pentanol. Its main formation pathway is H-abstraction by an iso-butyl radical ($i\dot{C}_4H_7$) on the fuel molecules. In *n*-butanol pyrolysis, $i\dot{C}_4H_7$ is mainly produced by recombination of an allyl radical ($\dot{C}_3H_5$-a) and an ethyl radical, leading to 1-pentene. In addition to the decomposition reaction to butadiene and a methyl radical described above, a 1-pentenyl radical can also dehydrogenate through $\beta$-scission reactions to form pentadiene ($C_5H_8$) and a $\dot{H}$


https://dx.doi.org/10.1021/acs.energyfuels.0c02252
*Energy Fuels* 2020, 34, 14708−14725

atom. The addition/elimination reaction of an ethyl radical ($\dot{C}_2H_5$) and pentadiene ($C_5H_8$) produces propene ($C_3H_6$) and an *iso*-butyl ($i\dot{C}_4H_7$) radical. The higher formation of iso-butene in *n*-pentanol pyrolysis is justified by higher yields of 1-pentene.

**3.2. Combustion of *n*-$C_3$−$C_6$ Alcohols.** *3.2.1. n-Butanol, n-Pentanol, and n-Hexanol Oxidation in Jet-Stirred Reactors.* Figure 4 compares experimental and predicted mole fractions for the three alcohols at temperatures from 500 to 1100 K at $p$ = 107 kPa. For brevity, we report detailed results only for the $\varphi$ = 1.0 case. The CRECK mechanism predicts experimental conversions satisfactorily for *n*-butanol and *n*-pentanol. No evidence of low-temperature reactivity emerges from the experimental observation for these two fuels, and the onset of conversion occurs only at ≈800 K. Some conversion is instead detected at $T$ = 620 K for *n*-hexanol, as expected based on its higher reactivity induced by the longer carbon chain available for low-temperature branching pathways. Simulations show that, after a limited conversion (≈20%) at $T$ = 620−640 K, reactivity begins again at ≈800 K for *n*-butanol and *n*-pentanol. The experimental results indicate a notable conversion below 800 K, making the onset of the high-temperature reactivity less steep compared to *n*-butanol and *n*-pentanol. While the same trend is observed for oxygen conversion, the formation of products starts only at 800 K, with the exception of *n*-hexanal, which is the only product carrying the fuel carbon backbone formed in significant quantities (i.e., 200 ppm, corresponding to 20% of fuel conversion) at lower temperatures. Analyzing the simulated conversion profiles, the CRECK model predicts two separate peaks for *n*-hexanal at the low- and high-temperature regimes, rather than a continuous and smoother profile. The same two-peak behavior is predicted for smaller aldehydes (formaldehyde, acetaldehyde, propanal, pentanal) and acetic acid. Such peaks arise from both the branching decomposition of the CHHP deriving from *n*-hexanol at low temperatures and from the Korcek decomposition of $C_6$ ketohydroperoxides (KHYP) formed through the reaction $\alpha\dot{Q}OOH + O_2 = H\dot{O}_2 + C_nKHYP$, as discussed in Section 2.10 of Part I.[1] In an attempt to find solutions to these shortcomings, we decreased the rate for CHHP decomposition by increasing the activation energy by 2 kcal mol$^{-1}$, in line with the values proposed in previous studies for long-chain alcohol fuel oxidation.[21−23] As a result, the onset of LT reactivity shifts by approximately 30 K toward higher temperatures, leaving the maximum conversion of *n*-hexanol unchanged.

The high-temperature formation of the corresponding $C_n$ aldehydes (butanal, pentanal, and hexanal) is associated with $\alpha$ radical chemistry. Both their interactions with $O_2$, forming $H\dot{O}_2$ radicals, and $\beta$-decomposition reactions involving the breaking of the O−H bond in the hydroxyl group contribute to this.

$C_n$ olefins are mainly produced by the $\beta$-decomposition reactions of secondary $\beta$ radicals ($R-\dot{C}_\beta H-C_\alpha H_2-OH$), producing $\dot{O}H$ radicals. Dehydration reactions and recombination of a methyl radical and resonantly stabilized radicals of the $C_{n-1}$ olefins (propene, butane, pentene) also contribute to the formation of the corresponding alkenes. The model largely overestimates the formation of cyclopentene ($cyC_5H_8$) and pentadienes ($C_5H_8$) for *n*-pentanol and *n*-hexanol oxidation, supporting the need of revising the subsets describing the pyrolysis and oxidation of pentene isomers.[24−26] Indeed, the model strongly underestimates the formation of pentenes from *n*-pentanol, but it agrees very well with the corresponding species in *n*-butanol and *n*-hexanol (i.e., butene and hexene).

$C_{n-1}$ olefins derive from the $\beta$-decomposition reactions of secondary $\gamma$ radicals ($R-\dot{C}_\gamma H-C_\beta H_2-C_\alpha H_2-OH$) decomposing into $\dot{C}H_2OH$ and $C_{n-1}$ alkene, by breaking the $C_\beta-C_\alpha$ bond of the $C_n$ alkyl radical. Overall, very good agreement is obtained for *n*-butanol and *n*-pentanol. More significant deviations are observed for *n*-hexanol oxidation. In addition to the differences mentioned above for the low-temperature regime, the model largely overpredicts methane ($CH_4$) yields. Most of the reactions governing methane formation and consumption belong to the core chemistry,[27−30] whose revision is beyond the scope of this study. Some minor influence of $\beta$-scission reactions producing methyl radicals ($\dot{C}H_3$) can be observed based on the rate of production analysis. Ethylene is underpredicted by a factor of ≈1.5 in the case of *n*-hexanol. Sensitivity and flux analyses highlight the major role of the reactions belonging to the $C_2/C_3$ portion of the present model in producing and/or consuming ethylene. Modifications in the rate parameters of reactions such as $\dot{C}_2H_5 + O_2 = H\dot{O}_2 + C_2H_4$ or $n\dot{C}_3H_7 (+M) = \dot{C}H_3 + C_2H_4 (+M)$ are outside the scope of this study. Acetylene, formed by successive reactions of unsaturated enols (butenol, pentenol, hexenol) and aldehydes (butenal-$C_3H_5CHO$, pentenal-$C_4H_7CHO$, hexenal-$C_5H_9CHO$), is strongly overpredicted in the case of *n*-hexanol. However, it is reasonable to expect that higher yields of acetylene should be produced from longer carbon chain fuels, at least for richer conditions, as it is predicted by the kinetic model (Figures S5, S6, S12, and S13).

Successive oxidation and decomposition reactions of $C_n$ aldehydes are responsible for acrolein ($C_2H_3CHO$) formation. Recombination of resonantly stabilized radicals ($\dot{C}_3H_5$-a, $\dot{C}_4H_7$1-3, $\dot{C}_5H_9$1-3, etc.) with $H\dot{O}_2$, forming $\dot{O}H$ and an alkoxy radical, governs acrolein formation in the JSR both at atmospheric pressure, where it is overpredicted, and at higher pressure ($p$ = 10 bar), where it is underpredicted (see Figure 7). Overall, any modification of the acrolein formation pathways will not lead to any global improvement. Moreover, the chemistry of aldehydes and related intermediates such as acrolein has recently been discussed and validated,[12] with modifications outside the scope of this study. However, a deeper knowledge of the kinetics involving unsaturated aldehyde and alcohol (enol) pyrolysis and oxidation would be beneficial to improve the agreement with the speciation targets presented in Figure 4.

A rate of production analysis was performed at $T$ = 825 K, $p$ = 1 bar, and $\varphi$ = 1 for the three fuels (Figure 5).

As expected from the increasing molecular weight, at $T$ = 825 K, the fuel conversion ($\chi$) is as follows: *n*-butanol ($\chi$ = 18%) < *n*-pentanol ($\chi$ = 19%) < *n*-hexanol ($\chi$ = 25%). *n*-Butanol is mostly consumed by H-atom abstraction by $\dot{O}H$ and $H\dot{O}_2$ radicals from the $\alpha$ position, forming $\dot{R}_{(A)}$ (49%) and from the alkane-like moiety, forming $\dot{R}_{(B)}$ (47%). Only 4% of the fuel consumed forms alkoxy ($R\dot{O}$) radicals. The $\alpha$ radical mostly forms the corresponding aldehyde (*n*-butanal) and $H\dot{O}_2$ radicals. Small reactive fluxes (4%) are associated with $\beta$-decomposition reactions, forming ethenol, which rapidly converts into acetaldehyde via tautomerization, and with isomerization reactions transferring a H-atom from the alkane-like moiety and increasing the yields of $\dot{R}_{(B)}$. This radical addition to $O_2$ (16%), with the possible onset of low-temperature chain branching pathways, competes with $\beta$-decomposition reactions (23%), mostly forming olefins (butene and propene) together with hydroxyl or hydroxyl-methyl radicals ($\dot{O}H$, $\dot{C}H_2OH$). 6% of the flux-producing $RO_2$ undergoes backward decomposition


https://dx.doi.org/10.1021/acs.energyfuels.0c02252
Energy Fuels 2020, 34, 14708−14725

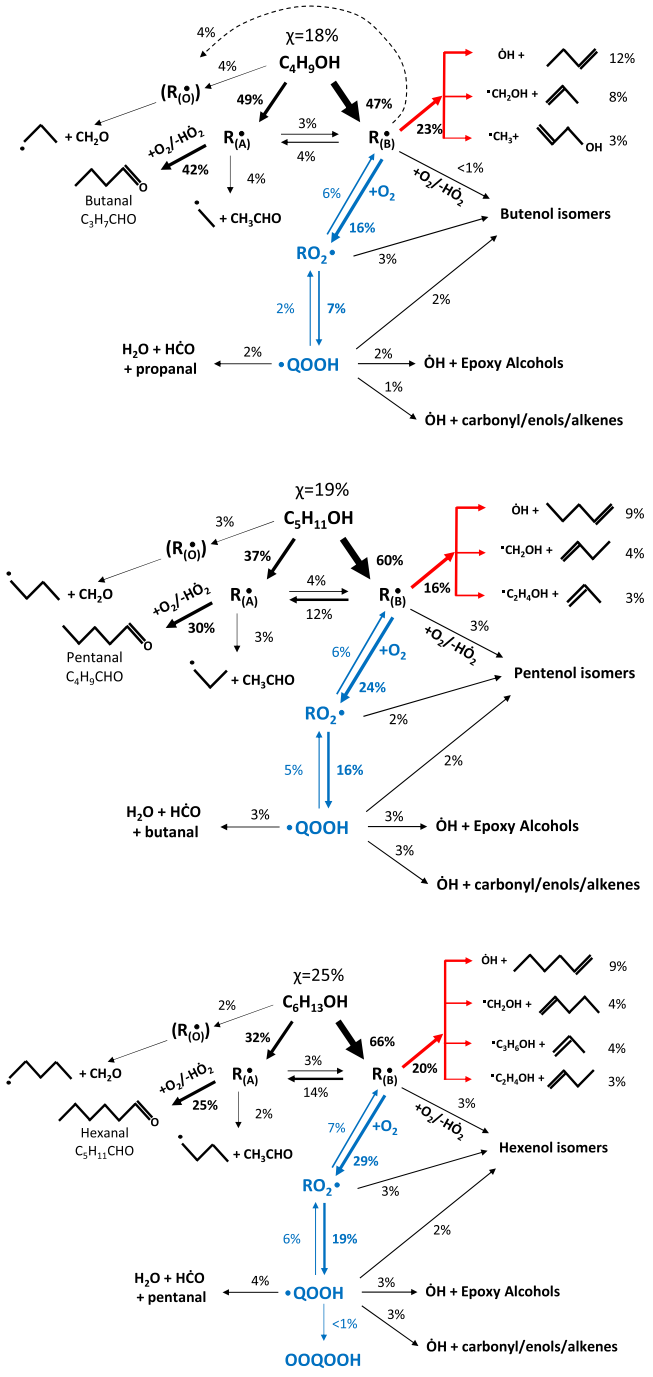


**Figure 5.** Rate of production analysis of n-butanol ($C_4H_9OH$), *n*-pentanol ($C_5H_{11}OH$), and *n*-hexanol ($C_6H_{13}OH$) oxidation in a jet-stirred reactor at $T$ = 825 K, $p$ = 1 bar, and $\varphi$ = 1. The threshold is set to 2%.

into $\dot{R}$ + $O_2$, 7% isomerizes to $\dot{Q}OOH$, and the remaining 3% decomposes to form butenol isomers and $H\dot{O}_2$. As expected, due to the relatively low-pressure condition, the second addition of $\dot{Q}OOH$ to $O_2$ is not favored and dehydration or decomposition reactions to unsaturated species (olefins, carbonyl, and unsaturated alcohols) and $\dot{O}H$ or to epoxy alcohols and $\dot{O}H$ dominate, inhibiting the low-temperature reactivity. As the chain length of the fuel increases, the relative importance of the alkane-like moiety for H-atom abstraction reactions increases. Consistent with *n*-butanol, $\dot{R}_{(A)}$ mostly produces *n*-pentanal in *n*-pentanol oxidation. 24% of $\dot{R}_{(B)}$ undergoes oxygen addition, and 20% decomposes through $\beta$-scission reactions to produce olefins and hydroxyl or hydroxyalkyl radicals ($\dot{O}H$, $\dot{C}H_2OH$, $\dot{C}_2H_4OH$). Isomerizations to $\dot{R}_{(A)}$ are more favored in *n*-pentanol oxidation (14%), as expected due to the higher importance of the six-membered isomerization reactions having a lower ring-strain energy. A net flux of 18% reaches $\dot{Q}OOH$ that once again preferentially decomposes into decomposition products via $\beta$-decomposition or dehydration reactions. Similar observations can be applied to *n*-hexanol, where the higher selectivity to the alkane-like moiety of H-atom abstractions and more favored isomerization reactions push the low-temperature branching pathways toward the second addition to $O_2$, forming $\dot{O}_2QOOH$ that mostly isomerizes to CHHP. Despite the very limited flux (i.e., <1% of the initial fuel), CHHP decomposition contributes to chain branching, increasing the radical pool and enhancing fuel conversion.

A synopsis of the JSR results at the three different equivalence ratios is reported in Figure 6 for the three fuels. In addition to the comparisons for fuel conversion and CO, $CH_2O$ and $C_n$ aldehyde formation summarized in Figure 6, detailed results for $\varphi$ = 0.5 and 2.0 are provided in Figures S5 and S6 of the Supporting Information. The model generally shows good agreement in terms of fuel conversion and major species profiles, as also documented also in the Supporting Information. The low-temperature reactivity of *n*-hexanol is significantly over-predicted for the lean case ($\varphi$ = 0.5). Unfortunately, ad hoc modifications to the kinetic model aimed at improving the agreement in this specific case would have impacted negatively the results for IDT simulations reported in Section 3.2.2. Moreover, the model correctly reproduces *n*-hexanol conversion at $\varphi$ = 0.5 for the speciation measurements at $p$ = 10 bar (Figure S12). As a further check, we performed model simulations for *n*-pentane oxidation[31] at the same conditions as those for the atmospheric pressure JSR experiments. Indeed, the alcohol-specific function does not influence the low-temperature reactivity of the carbon chain farther away from the $\alpha$ site. In other words, *n*-hexanol can be loosely assumed to be equivalent to *n*-pentane, by substituting the $CH_2$−OH function with one H atom. Figure S39 in the Supporting Information supports this assumption as *n*-hexanol and *n*-pentane show very similar reactivity in the low-temperature/NTC range. This observation together with the satisfactory agreement with other experimental targets discussed in the following sections increases, to some extent, the confidence in the reliability of our model. For example, sensitivity analyses highlight that the second addition to $O_2$ ($\dot{Q}OOH$ + $O_2$) and H-atom abstraction reactions leading to the lumped radical ($\dot{B}$) enhance the conversion of *n*-hexanol. Therefore, a reduction to these rate constants would be needed to improve model performances for the JSR cases. Unfortunately, this is in conflict with the sensitivity analysis to IDT predictions (see Figure 12). Indeed, the same reactions show positive sensitivity coefficients, meaning that a rate constant reduction would compromise the good agreement highlighted for *n*-hexanol/air IDTs (see Figure 10), making them too slow.

The oxidation of *n*-butanol, *n*-pentanol, and *n*-hexanol was also investigated in the JSR at CNRS-Orléans.[22,23,32] Experimental data have been systematically obtained over the last decade for highly diluted mixtures of 1000 ppm of fuel in $O_2$ and $N_2$, at $\varphi$ = 0.5, 1.0, and 2.0. The reactor is operated at $p$ = 10 bar, in the temperature range $T$ = 550−1150 K for *n*-hexanol and $T$ = 750−1150 K for *n*-butanol and *n*-pentanol, with residence time $\tau$ = 0.7 s. Similar data for *n*-propanol (1500 ppm in $O_2/N_2$, $\varphi$ = 0.25, 0.5, 1.0, 2.0) have been reported by Galmiche et al.[33] In


https://dx.doi.org/10.1021/acs.energyfuels.0c02252
Energy Fuels 2020, 34, 14708−14725

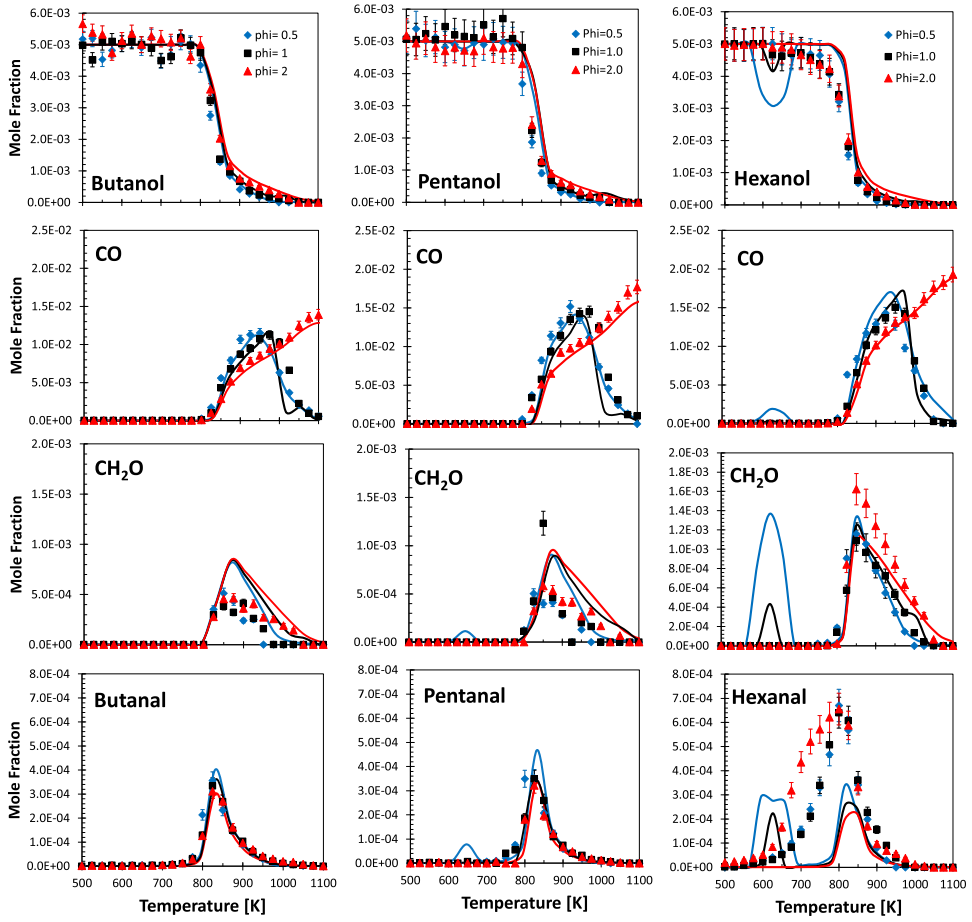


**Figure 6.** *n*-butanol, *n*-pentanol, and *n*-hexanol oxidation in JSR at $\varphi$ = 0.5, 1.0, and 2.0, $p$ = 107 kPa, and $\tau$ = 2.0 s. Comparison between experimental (symbols) and predicted (lines) fuel conversion and mole fraction profiles for selected intermediate and product species. A complete comparison for $\varphi$ = 0.5 and 2.0 is provided in Figures S5 and S6 of the Supporting Information.

addition, Sarathy et al.[21] reported experimental data at $p$ = 1 bar in the same reactor for *n*-butanol. The reacting mixtures were probe-sampled by means of a fused silica low-pressure sonic probe. The samples were analyzed online by FT-IR and offline after collection and storage in 1 L Pyrex bulbs. Offline analysis was done using GCs equipped with capillary columns (DB-624 and Carboplot-P7), a TCD, and an FID (flame ionization detector).

Figure 7 compares model predictions and experimental data for *n*-butanol, *n*-pentanol, and *n*-hexanol at $\varphi$ = 1.0 and $p$ = 10 bar, providing insights into the relative reactivity of the three fuels. Additional comparisons for leaner and richer mixtures are reported in the Supporting Information (Figures S12 and S13). The simulations using the present model are also compared to the data of Galmiche et al.[33] for *n*-propanol oxidation in Figures S8−S11 and with the atmospheric pressure data for *n*-butanol[21] in Figures S14−S17.

The model correctly reproduces the consumption of the fuels and the onset of reactivity, particularly at $T$ > 750 K. The low-temperature reactivity of *n*-hexanol ($T$ = 550−750 K) seems to be slightly overestimated by looking at the *n*-hexanol mole fraction profile as the experimental data do not show any clear fuel conversion due to low-temperature branching pathways. However, some intermediate species representative of low-temperature branching pathways, such as CHHP decomposition reactions forming $CH_2O$ and $CH_3CHO$, are experimentally detected and the model reproduces their peak formation within experimental uncertainty. By looking at the experimental mole fraction of *n*-hexanol, it is possible to observe some uncertainty in the fuel concentration at $T$ < 750 K. Indeed, the nominal concentration of 1000 ppm is exceeded by at least 10%, thus resulting in an overall higher equivalence ratio $\varphi$ inhibiting the low-temperature reactivity. The capability of the model to correctly reproduce the low temperature oxidation of *n*-hexanol is further supported by the comparison with the $\varphi$ = 0.5 data reported in the Supporting Information (Figure S12). Similar uncertainties in experimental fuel mole fraction are observed for the $\varphi$ = 2.0 data set (Figure S13), explaining the deviations of the model predictions. For a more significant comparison with *n*-butanol and *n*-pentanol data, the mole fraction of the fuel in the reactor feed was kept at the nominal value of 1000 ppm.

The main oxidation products (CO, $CO_2$, and $H_2O$) are correctly reproduced by the model for the three fuels. Differently from the comparisons of Figure 4, methane ($CH_4$) formation is slightly under-estimated (≈15−20%) for *n*-butanol and *n*-pentanol. A slight overestimation (≈10%) is instead persisting for *n*-hexanol. At $T$ > 850 K, propene ($C_3H_6$) is mainly produced by $\beta$-decomposition reactions of secondary radicals adjacent to the terminal methyl group in the alkane-like moiety. The same reactions govern propene formation in the JSR experiments presented in Figure 4, where the model captures the experimental profiles very well. Ethylene ($C_2H_4$) is nicely reproduced for *n*-butanol and underestimated by a factor of ≈2 for *n*-pentanol and *n*-hexanol, confirming for the latter two fuels


https://dx.doi.org/10.1021/acs.energyfuels.0c02252
*Energy Fuels* 2020, 34, 14708−14725

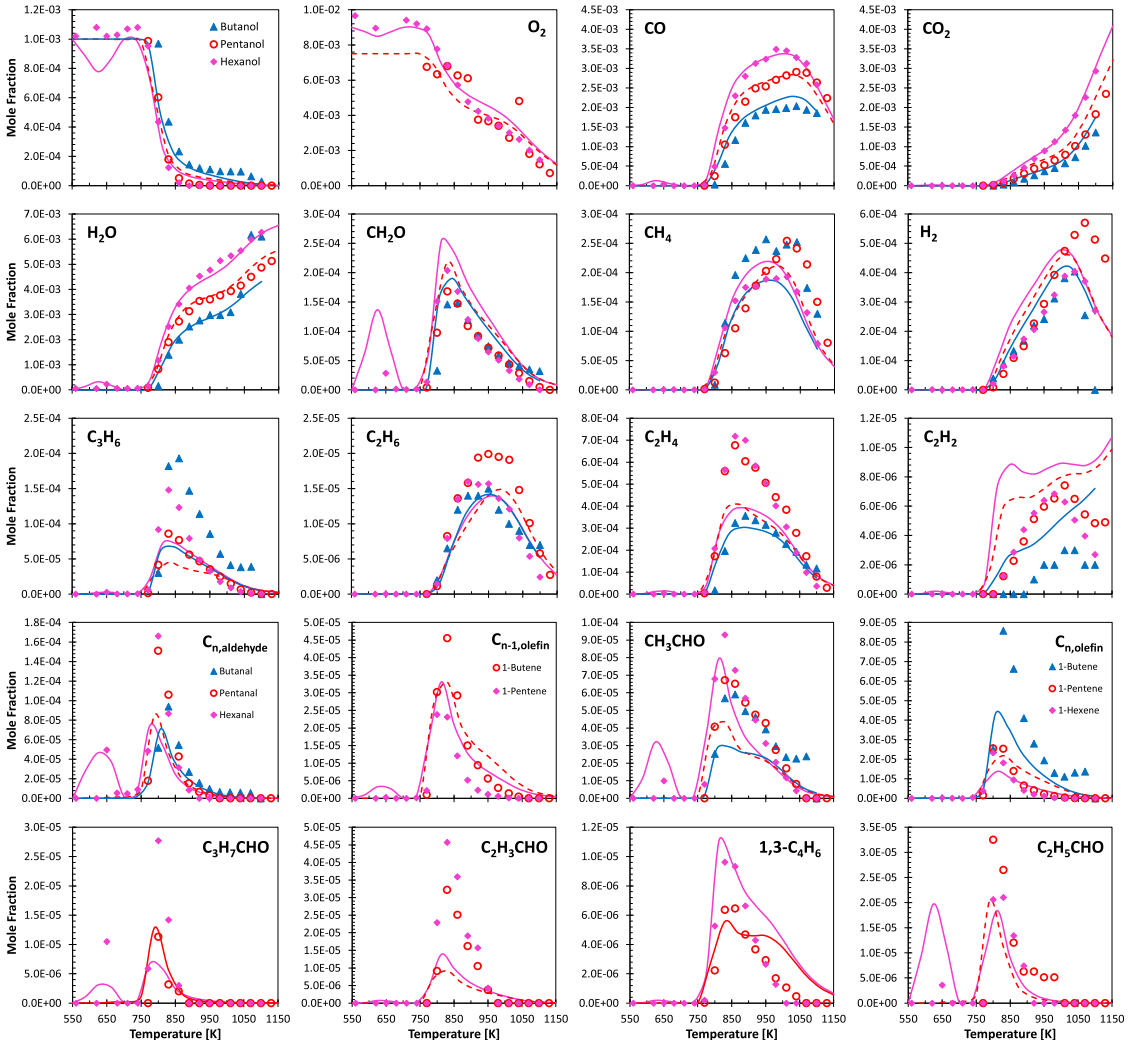


**Figure 7.** *n*-butanol, *n*-pentanol, and *n*-hexanol oxidation in JSR at $\varphi$ = 1.0, $p$ = 10 bar, and $\tau$ = 0.7 s. Comparison between experimental (symbols)[22,23,32] and predicted (lines) mole fraction profiles of intermediate and product species.

the deviations observed for the atmospheric pressure cases. Peak concentrations of the corresponding $C_n$ aldehyde derived from the interaction of $\alpha$ radicals with $O_2$ in the higher-temperature conditions are correctly predicted for *n*-butanol (i.e., butanal-$C_3H_7CHO$ profile) and underestimated by a factor of ≈1.5 for *n*-pentanol (i.e., pentanal-$C_4H_9CHO$ profile) and *n*-hexanol (hexanal-$C_5H_{11}CHO$ profile). Similar deviations have been observed for *n*-hexanal at atmospheric pressure conditions (Figure 4). Good agreement is observed for the formation of $C_n$ alkenes (1-butene, 1-pentene, 1-hexene), mostly derived from $\beta$-decomposition reactions of secondary $\beta$ radicals, with the exception of 1-butene, which is underestimated by approximately a factor of 2. $C_{n-1}$ olefins in *n*-pentanol and *n*-hexanol oxidation are formed through $\beta$-scission reactions of secondary $\gamma$ radicals. Similarly to the atmospheric pressure case, the simulations using the present model satisfactorily reproduce the experimental data. Small amounts (<30 ppm) of lower-molecular-weight aldehydes ($C_3H_7CHO$ and $C_2H_5CHO$) in *n*-pentanol and *n*-hexanol oxidation are formed through the decomposition reactions of $\dot{Q}OOH$ radicals through dehydration reactions (Reaction Class 15[1]) or via the Waddington mechanism (Reaction Class 11[1]). Acetaldehyde is formed through $\beta$-decomposition reactions of $\alpha$ radicals to ethenol and successive tautomerizations. The higher-temperature peak of formaldehyde is related to the oxidation reaction of ethanol primary radical ($O_2 + \dot{C}_2H_4OH \leftrightarrow \dot{O}_2C_2H_4OH \leftrightarrow CH_2O + CH_2O + \dot{O}H$). The analysis in Figure 8 compares reactive fluxes for *n*-pentanol oxidation at the conditions measured in the Nancy JSR (Figure 4) and at Orléans (Figure 7).

The main difference is associated with a higher flux reaching CHHP branching decomposition in the higher-pressure case, as expected from the promoting effect of pressure on first and second addition reactions. Other differences related to the fuel conversion have to be referred to different fuel concentrations obtained from the different pressure conditions and different fuel mole fractions. The concentration of *n*-pentanol in the higher-pressure case is indeed five times higher than for the atmospheric pressure conditions. This effect is partly counterbalanced by a lower residence time $\tau$ (i.e., 0.7 s at 10 bar, 2.0 s at 1 bar).

*3.2.2. Ignition Delay Times in a Shock Tube and a Rapid Compression Machine.* This section compares IDT data from the literature[34−40] and from this work with model predictions. Only a limited number of data sets are discussed here, and additional validation targets[41−44] are reported in the Supporting Information (Figures S19−S29).

IDTs for mixtures of 0.5% mol fuel in $O_2$ and argon have been measured in low-pressure shock tubes at $T$ = 1250−1650 K, $p$ =


https://dx.doi.org/10.1021/acs.energyfuels.0c02252
Energy Fuels 2020, 34, 14708−14725

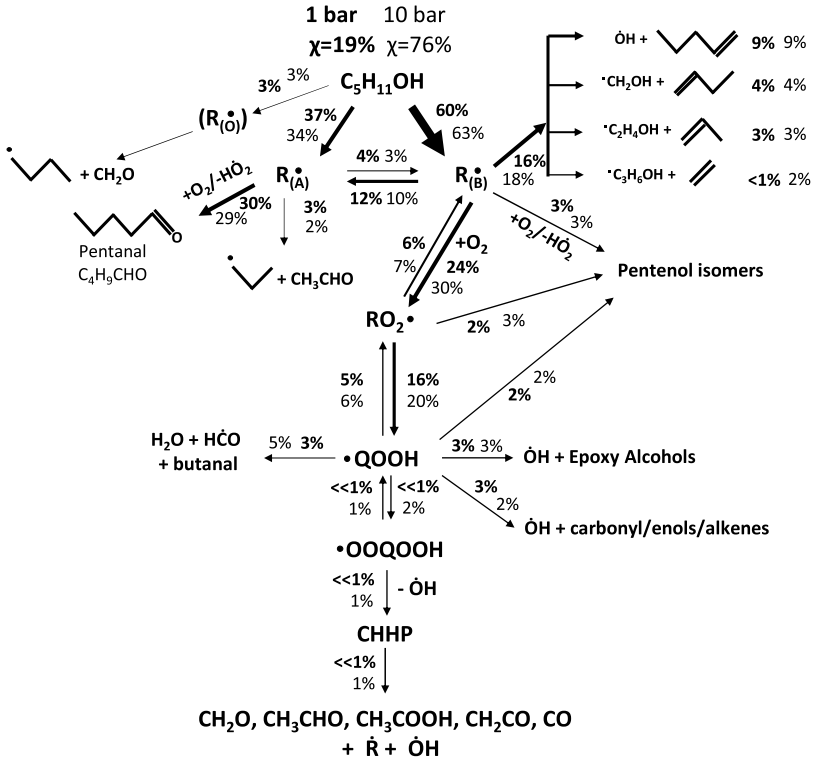


**Figure 8.** Rate of production analysis of n-pentanol ($C_5H_{11}OH$) oxidation in a jet-stirred reactor at $T$ = 825 K, $p$ = 1 bar, $\tau$ = 2.0 s, and $x_{fuel}$ = 0.5% mol (bold) and $p$ = 10 bar, $\tau$ = 0.7 s, $x_{fuel}$ = 0.1% mol (italics), and $\varphi$ = 1. The threshold is set to 2%.

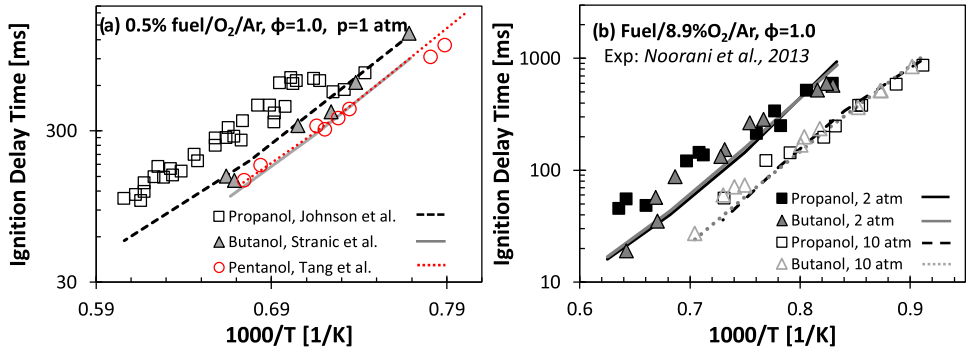


**Figure 9.** Shock-tube experimental (symbols)[34−37] and simulated (lines) IDTs for highly diluted mixtures (>90%) of *n*-propanol, *n*-butanol, and *n*-pentanol in $O_2$ and argon at high temperatures. Panel (a): $p$ = 1 atm, 0.5% mol fuel. Panel (b): $p$ = 2 and 10 atm, 8.9% $O_2$.

1 atm by Johnson et al.[34] (*n*-propanol), Stranic et al.[35] (*n*-butanol), and Tang et al.[37] (*n*-pentanol). Experimental data at $\varphi$ = 1.0 are compared with model results in Figure 9a. Additional comparisons for different dilution conditions are provided in the Supporting Information. The model correctly predicts the IDTs of *n*-pentanol but slightly underestimates (30−40%) the IDTs measured by Stranic et al. for *n*-butanol. Deviations up to a factor of ≈2 at very high temperatures ($T$ > 1600 K) are observed for *n*-propanol. Different apparent activation energies for ignition are observed for the three alcohols, while similar slopes are observed in the model predictions. Different experimental setups and procedures might partly justify the observed differences. Moreover, the model predicts very similar IDTs for *n*-butanol and *n*-pentanol, while, in agreement with the experimental data, *n*-propanol shows longer IDTs. The IDTs correlate with oxygen concentration, which is known to promote ignition at high temperatures. Having assigned a fuel mole fraction (0.5% mol in this case), the longer the carbon chain, the higher the amount of oxygen, the shorter the IDT. While this is evident for *n*-propanol, this effect is partly counterbalanced for *n*-butanol and *n*-pentanol by looking at the radical yields. For example, *n*-butanol produces more Ḣ atoms and fewer methyl radicals ($\dot{C}H_3$), thus enhancing the impact of the branching reaction Ḣ + $O_2$ = Ö + ȮH, which dominates the rate of high-temperature oxidation. This originates from the fate of fuel radicals and, for example, the fate of $\alpha$ radicals whose formation is highly favored, as discussed in previous sections. While *n*-butanol $\alpha$ radicals decompose into ethenol and ethyl radicals, those for *n*-pentanol decompose into ethenol and *n*-propyl radicals. Ethyl radicals undergo $\beta$-scission to form Ḣ atoms and ethylene, while *n*-propyl radicals form less reactive methyl radicals and ethylene. Similar observations have been reported in previous studies.[45,46]

A systematic investigation of $C_1$−$C_4$ primary alcohols has been reported by Noorani et al.[36] over the temperature range $T$ = 1070−1760 K, at pressures of 2 and 10 atm, for different oxygen/argon ratios and equivalence ratios. Results for


https://dx.doi.org/10.1021/acs.energyfuels.0c02252
Energy Fuels 2020, 34, 14708−14725

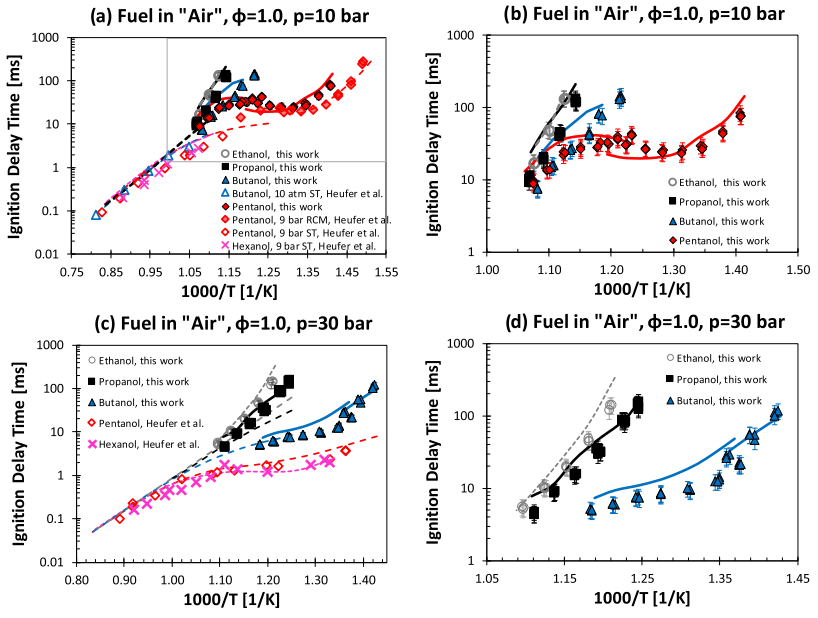


**Figure 10.** Experimental (symbols) (this work, Heufer et al.[38−40]) and simulated IDTs for stoichiometric fuel/air mixtures in STs (dashed lines, open symbols) and RCMs (solid lines, full symbols) at $p$ = 10 bar and 30 bar. Panels (b) and (d) show only the experimental data from this study (error bars = 25%).

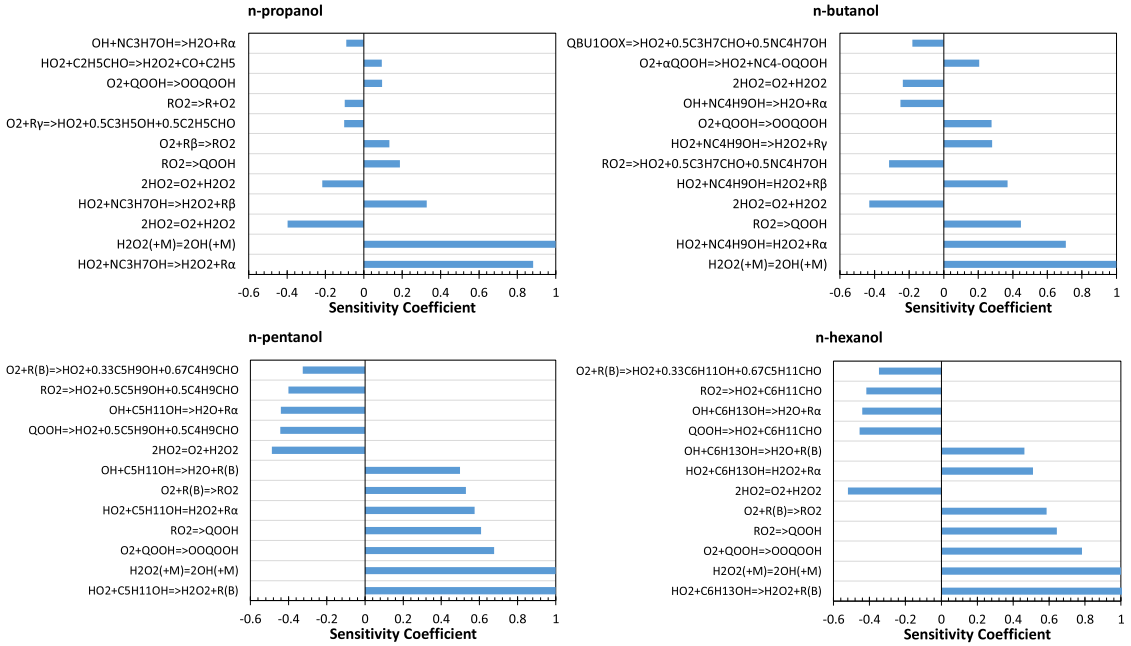


**Figure 11.** Sensitivity analysis of IDTs to rate constants for stoichiometric $n$-$C_3$−$C_6$ alcohols/air mixtures at $T$ = 900 K and $p$ = 10 bar.

stoichiometric conditions and 8.9% mol $O_2$ for $n$-propanol and $n$-butanol are shown in Figure 9b. The model agrees with the experiments in predicting very similar IDTs for the two fuels. Very good agreement is observed for the higher-pressure case, while deviations up to a factor of 2.5 are observed for the higher temperature in the case of $n$-propanol. It should be noted that a similar degree of deviation is highlighted by comparing the two atmospheric pressure data sets for IDTs lower than 100 $\mu$s. Higher uncertainties might be associated with very small IDTs in ST experiments due to boundary layers effects.[47] To highlight the reasons for the deviations observed for $n$-propanol, we performed a sensitivity analysis at $T$ = 1450 K for the lower-pressure case (i.e., 2 atm) of Figure 9b. Results are reported in Figure S37 of the Supporting Information. The initiation reaction, $nC_3H_7OH = \dot{C}H_2OH + \dot{C}_2H_5$, for which we selected a rate constant different from the rate rule (see Part I,[1] Section 2.2), is the most important reaction promoting ignition. H-atom abstractions by $\dot{H}$ and $\dot{O}H$ forming the $\alpha$ radical ($CH_3CH_2\dot{C}HOH$) and the dehydration reaction inhibit ignition. As a test, we adopted the same rate constant from the rate rules for the initiation reaction and recomputed the pyrolysis speciation data and the IDTs. Results are reported in Figure S38 of the Supporting Information. Reducing the rate of initiation improves IDT predictions at high temperatures and has a negative impact on $n$-propanol conversion profiles in the pyrolysis experiments. These observations highlight the need for


https://dx.doi.org/10.1021/acs.energyfuels.0c02252
Energy Fuels 2020, 34, 14708−14725

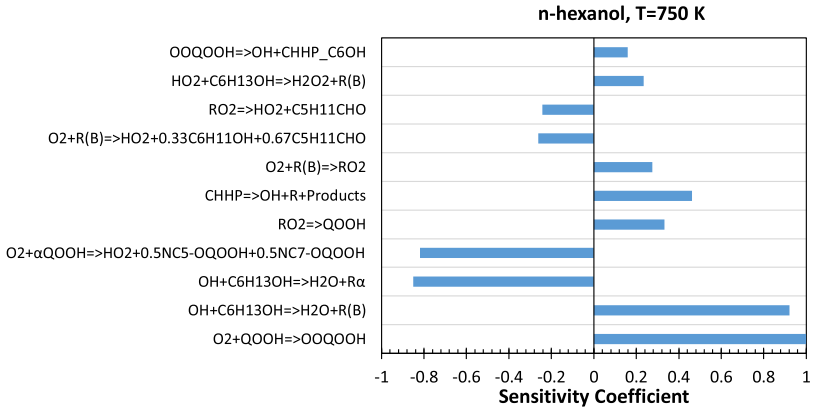


**Figure 12.** Sensitivity analysis of IDTs to rate constants for a stoichiometric n-hexanol/air mixture at $T$ = 750 K and $p$ = 10 bar.

a systematic investigation of unimolecular initiation reactions so as to facilitate the determination of more appropriate rate rules for this class of reaction.

Figure 10a,c compares experimental IDTs for stoichiometric ($\varphi$ = 1.0) fuel/air mixtures of $n$-$C_3$−$C_6$ alcohols in STs[39,40,48] and RCMs (this work and ref[38]) at $p$ = 10 and 30 bar with CRECK model predictions. Figure 10b,d shows only the comparison with the experimental measurements obtained in this work using the RCM at NUIG. Compositions of the mixtures and operating conditions for the new data are reported in Table 1. ST simulations have been carried out using an adiabatic constant volume batch reactor, accounting for the average pressure rise behind the reflected shock wave reported in the referenced experimental studies.[39,40,48] RCM simulations have been performed accounting for the volume histories as obtained from nonreactive experiments (Section 2). The model correctly reproduces temperature and pressure effects, as well as the different reactivity of the different fuels. The IDTs of the investigated fuels converge for $T$ > 900 K, while clear differences are observed for lower temperatures. In particular, $n$-hexanol is the most reactive, followed by $n$-pentanol, and $n$-butanol as expected from the longer carbon chain length enhancing the low-temperature branching pathways and limiting the influence of the alcohol-specific moiety that does not contribute to low-temperature reactivity. This observation is consistent with the discussion on the ignition propensity (CN and ON) in Part I.[1]

Moving from the lowest to the highest temperatures, differently from JSR experiments, it is possible to see for longer-chain alcohols (>$C_4$) the expected negative temperature coefficient (NTC) behavior widely observed for alkane fuels.[5,49−51] No NTC behavior is observed for ethanol and propanol at both pressures, and for $n$-butanol at $p$ = 10 bar. Higher pressures indeed enhance the low-temperature reactivity by favoring radical additions to $O_2$ or increasing the ceiling temperature, thus promoting the low-temperature branching pathways. A clear NTC behavior is only observed for the $n$-pentanol and $n$-hexanol/air mixtures at $p$ = 30 bar, while the increased importance of low-temperature reactions results in an evident slope change for the $n$-butanol/air mixture.

Maximum deviations of a factor of ≈1.5 are observed for the ST experiments and for the RCM data at $p$ = 30 bar. Slightly higher deviations (factor of ≈2) are observed for the RCM experiments at $p$ = 10 bar.

Figure 11 shows results from a sensitivity analysis carried out for stoichiometric fuel/air mixtures at $T$ = 900 K and $p$ = 10 bar. Details of the sensitivity analysis methodology have been discussed by Cuoci et al.[14] Sensitivity coefficients thus obtained have been normalized on the decomposition reaction of hydrogen peroxide $H_2O_2$ (+M) = $\dot{O}H$ + $\dot{O}H$ (+M) that is well known to be responsible for the transition to the high-temperature ignition regime at such conditions. A positive coefficient stands for a reaction-enhancing ignition. In general, H-atom abstraction reactions by $H\dot{O}_2$ forming $H_2O_2$ promote reactivity as hydrogen peroxide is rapidly decomposed to form two $\dot{O}H$ radicals. These H-atom abstractions compete with $H\dot{O}_2$ self-recombination/disproportionation forming hydrogen peroxide and molecular oxygen, acting as a termination reaction and thus reducing reactivity. H-atom abstractions by $\dot{O}H$ forming $\dot{R}_\alpha$ are highlighted as reactivity inhibitors, despite lower absolute values, which is related to the predominance of $\dot{H}$ + $O_2$ (+M) = $H\dot{O}_2$ (+M) over $\dot{H}$ + $O_2$ = $\ddot{O}$ + $\dot{O}H$ at the investigated conditions. Note that $\alpha$ radicals mostly form $H\dot{O}_2$ and the corresponding aldehyde, thus triggering the competition between the above channels of the hydrogen oxygen system. Reactions belonging to the low-temperature branching pathway toward the formation of CHHP (e.g., $\dot{R}$ + $O_2$ ↔ $R\dot{O}_2$, $R\dot{O}_2$ ⇌ $\dot{Q}OOH$, $O_2$ + $\dot{Q}OOH$ ↔ $\dot{O}_2QOOH$) activate the system, despite their limited fluxes due to relatively high-temperature conditions. $\dot{Q}OOH$ radical decomposition reactions generally decrease the reactivity, with the exception of the interactions of $\alpha\dot{Q}OOH$ with $O_2$ forming $H\dot{O}_2$ and the ketohydroperoxide of the corresponding $C_n$ alkane, as its fast decomposition at $T$ = 900 K provides a branching effect. This reaction appears within the most sensitive reactions for $n$-butanol, $n$-pentanol, and $n$-hexanol.

Figure 12 shows the sensitivity analysis for $n$-hexanol at $T$ = 750 K scaled on the basis of the most sensitive reaction, i.e., the second addition to $O_2$ ($\dot{Q}OOH$ + $O_2$ ↔ $\dot{O}_2QOOH$). H-atom abstractions by $\dot{O}H$ govern the reactivity and in particular the relative selectivity to the formation of $\alpha$ radicals or alkyl radicals in the alkane-like moiety ($\dot{R}_{(B)}$). Notably, the reaction $\alpha\dot{Q}OOH$ + $O_2$ = $H\dot{O}_2$ + $C_n$KHYP has now a negative sensitivity coefficient, thus differently from higher temperatures ($T$ = 900 K, Figure 11), it inhibits reactivity. This feature calls for improved determinations of the rate constants for this channel, whose existence has been first proposed by Welz et al.[52] and for which we might be adopting a rather uncertain value. CHHP formation from $\dot{O}_2QOOH$ and its decomposition decreases IDTs. As already discussed in Section 3.2.1, it should be noted that, in the JSR experiments, the same reactions highlighted in Figure 12 also dominate $n$-hexanol oxidation. For this reason, it is not possible to improve the performances of the model in


https://dx.doi.org/10.1021/acs.energyfuels.0c02252
Energy Fuels 2020, 34, 14708−14725

Figures 6 and 7 without losing agreement for the *n*-hexanol/air IDT predictions.

*3.2.3. Extension to n-Octanol Oxidation.* As a further demonstration of the general validity of the proposed rate rules and of the lumping technique discussed in Part I of this study[1] the model has been extended to describe the pyrolysis and oxidation of *n*-octanol. The same lumped parameters determined for *n*-hexanol have been adopted to describe the low-temperature oxidation of *n*-octanol. The longer chain length has been properly accounted for in the description of unimolecular initiation reactions and H-atom abstraction reactions, to consider a higher number of bonds possibly undergoing homolytic fissions and for a higher number of sites available for H-atom abstractions. The same approach was already successfully applied[53] to describe the combustion of heavy *n*-alkanes.

Despite interest in it as a renewable fuel for diesel and jet engines,[54] the only data available in the literature are those presented by Cai and co-workers.[55] IDTs of stoichiometric *n*-octanol/air mixtures have been measured in a high-pressure shock tube in the temperature range $T$ = 720−1250 K at pressures of 20 and 40 bar. The same study presented speciation measurements at $T$ = 500−1150 K obtained in a JSR operating at $p$ = 10 bar for 1000 ppm *n*-octanol/$O_2$/$N_2$ mixtures at $\varphi$ = 0.5, 1.0, and 2.0. Figure 13 compares model predictions with the experimental IDT data. The model agrees with the experimental measurements within a factor of 1.25.

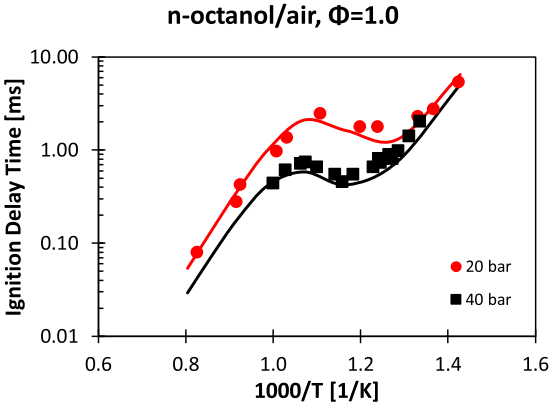


**Figure 13.** Ignition delay times of stoichiometric *n*-octanol/air mixtures at $p$ = 20 and 40 bar in a shock tube. Symbols: experimental measurements,[55] lines: model simulations.

Figure 14 compares model predictions with experimental data for the oxidation of *n*-octanol in a jet-stirred reactor.[55] As highlighted for the IDTs, *n*-octanol shows a pronounced NTC behavior also for the JSR measurements. Major species such as CO, $CO_2$, and $H_2O$ are well predicted for every equivalence ratio condition. The fuel reactivity in the low-temperature region is under-predicted by a factor of ≈2, with deviations similar to those observed by Cai et al.[55] Additional comparisons for other measured species are reported in the Supporting Information (Figures S34−S36).

*3.2.4. Laminar Flame Speed.* A number of experimental measurements of laminar flame speed for *n*-$C_3$−$C_6$ alcohols have been reported in the literature using various techniques.[16,17,22,23,45,56−68] Different unburned gas temperatures ($T$ = 343−600 K), pressures ($p$ = 1−10 atm), and equivalence ratios ($\varphi$ = 0.6−1.7) have been explored, providing a relatively high number of data for combustion model validation.

This is particularly true for *n*-propanol, *n*-butanol, and *n*-pentanol, with a more limited number of measurements available for *n*-hexanol. A sample set is reported in Figure 15, comparing the experimental laminar flame speeds of the different fuels at the same unburned gas conditions with model predictions. Air is assumed to be composed of 21% mol $O_2$ and 79% mol $N_2$. Additional comparisons are reported in the Supporting Information (Figures S30−S33). As evident in Figure 15 in addition to the large variability of the data from different sources at the same unburned gas conditions, no clear reactivity trends as a function of the carbon chain length are evident, while the model predicts an increasing laminar flame speed moving from *n*-propanol to higher-molecular-weight alcohols. At $T$ = 423 K and $p$ = 1 atm, the maximum laminar flame speed ($\varphi \approx 1.1$) predicted by the model is 68 cm $s^{-1}$ for *n*-propanol, 72 cm $s^{-1}$ for *n*-butanol, 73 cm $s^{-1}$ for *n*-pentanol, and 74 cm $s^{-1}$ for *n*-hexanol. The different measurements at the same conditions suggest an opposite trend, and the model shows overprediction as high as 10 cm $s^{-1}$ for *n*-hexanol. As discussed by Nativel et al.[45] assessing the uncertainty in different literature measurements for *n*-pentanol/air mixtures, most of these discrepancies might be associated with air composition. Laminar flame speeds showed variations of up to 7 cm $s^{-1}$ for oxygen concentrations ranging from 20.0 to 20.9% mol. For the case of *n*-butanol at $T$ = 423 K and $p$ = 1 atm in Figure 15, we also computed the laminar flame speed for different oxygen concentrations, i.e., 20.9 and 20.0%, confirming the strong effect of decreasing oxygen content, i.e., 7 cm $s^{-1}$ decrease of the peak flame speed.

Providing the observations above and considering that the large majority of the experimental studies do not specifically declare the exact composition of air, only a few datasets are matched by model simulations where we assumed 21% oxygen concentration. Moreover, it is also clear that more systematic experimental investigations for the different fuels, using the same facility, could provide at least qualitative guidelines for model improvement. This discussion also highlights once again the importance of exhaustive data reporting and the existing concerns for alcohol flame data reproducibility. In addition to the uncertainty related to air composition, other sources of experimental uncertainties are associated with different experimental methods, procedures, and setups. A deeper discussion of this topic as well as the revision of the core chemistry dominating laminar flame propagation is beyond the scope of this study.

## 4. CONCLUSIONS

*n*-$C_3$−$C_6$ alcohol combustion was experimentally investigated in a JSR and in an RCM. JSR data were obtained for *n*-butanol, *n*-pentanol, and *n*-hexanol at nearly atmospheric pressure (i.e., 107 kPa), in the temperature range $T$ = 550−1100 K and at equivalence ratios $\varphi$ = 0.5, 1.0, and 2.0. IDTs for stoichiometric fuel/air mixtures have been measured in a rapid compression machine at $p$ = 10 and 30 bar and $T$ = 704−935 K for ethanol, *n*-propanol, *n*-butanol, and *n*-pentanol (10 bar only). These data present the first comparative and systematic investigation of such fuels and provide precious validation targets for model development. In particular, to the best of our knowledge, we present the first experimental measurement for *n*-pentanol and *n*-hexanol oxidation at atmospheric pressure and the first high-pressure/intermediate-temperature IDT data in a rapid


https://dx.doi.org/10.1021/acs.energyfuels.0c02252
Energy Fuels 2020, 34, 14708−14725

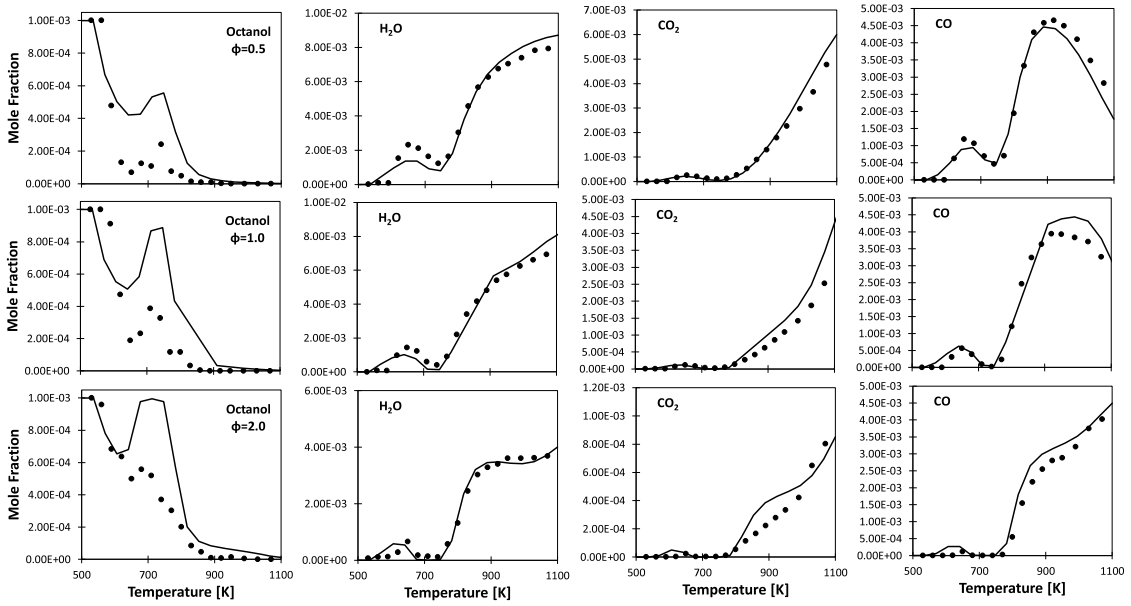


**Figure 14.** *n*-octanol oxidation in a jet-stirred reactor at $\varphi$ = 0.5, 1.0, and 2.0 at $p$ = 10 bar and $\tau$ = 0.7 s. Experimental data (symbols)[55] and model simulations (lines) for *n*-octanol and main product species mole fraction profiles.

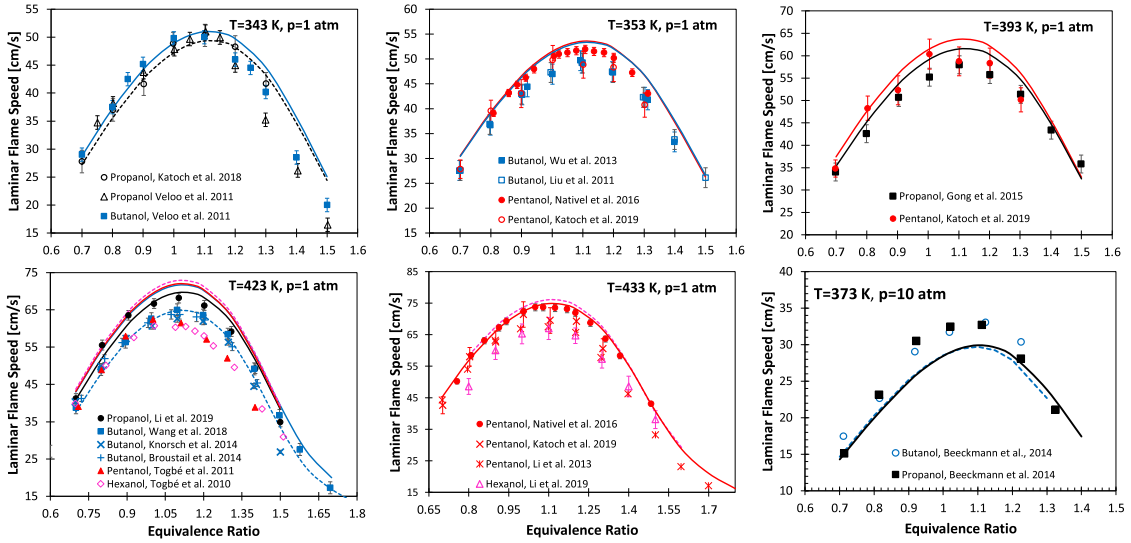


**Figure 15.** Experimental (symbols)[16,17,22,23,45,56−68] and simulated laminar flame speed of alcohol/air (21% $O_2$, 79% $N_2$ in mol) mixtures at different unburned gas temperatures and pressures. *n*-propanol: black, *n*-butanol: blue, *n*-pentanol: red and *n*-hexanol: pink. The case at $T$ = 423 K and $p$ = 1 atm also shows results for *n*-butanol/air considering 20% $O_2$ concentration in air (blue dashed line).

compression machine for *n*-propanol. With these new targets and considering the large amount of experimental information on pyrolysis and combustion available in the literature, the CRECK kinetic model described in Part I has been successfully validated and the robustness of its approach has been demonstrated by extending the same rate rules to describe *n*-octanol combustion. However, some non-negligible and non-systematic deviations have been observed for some experimental targets, posing some questions as to the validity of the rate-rule-based approach. In our opinion, uncertainties in both experimental measurements and model parameters should be considered. One of the major advantages of a rate-rule-based model development strategy, in particular when considering a large number of data for its validation, lies in the possibility of highlighting systematic deviations pointing to model shortcomings or to irreconcilable deviations among different experimental measurements.

The CRECK model attached to this study also describes the oxidation of other real fuel components (*n*-alkanes, *iso*-alkanes, aromatics, cyclo-alkanes, etc.) and the formation of pollutants (NOx, PAHs, soot), thus constituting a useful tool for fuel design.

## ■ ASSOCIATED CONTENT

### Supporting Information

The Supporting Information is available free of charge at https://pubs.acs.org/doi/10.1021/acs.energyfuels.0c02252.

Mixture compositions for RCM experiments; experimental ignition delay times; additional validation targets for $nC_3$-$C_6$ alcohols; *n*-octanol oxidation in a jet-stirred reactor; additional analyses (PDF)



https://dx.doi.org/10.1021/acs.energyfuels.0c02252
*Energy Fuels* 2020, 34, 14708−14725

Part2_volume_profiles_RCM (XLSX)
Part2_JSR_data_alcohols (XLSX)

## AUTHOR INFORMATION


### Corresponding Author

**M. Pelucchi** − *CRECK Modeling Lab, Department of Chemistry Materials and Chemical Engineering, Politecnico di Milano, 20133 Milano, Italy;* orcid.org/0000-0003-3106-0236; Phone: +39 02 2399 4234; Email: matteo.pelucchi@polimi.it

### Authors

**S. Namysl** − *Laboratoire Réactions et Génie des Procédés, CNRS, Université de Lorraine, ENSIC, 54000 Nancy Cedex, France*

**E. Ranzi** − *CRECK Modeling Lab, Department of Chemistry Materials and Chemical Engineering, Politecnico di Milano, 20133 Milano, Italy;* orcid.org/0000-0002-1395-6074

**A. Rodriguez** − *Laboratoire Réactions et Génie des Procédés, CNRS, Université de Lorraine, ENSIC, 54000 Nancy Cedex, France*

**C. Rizzo** − *CRECK Modeling Lab, Department of Chemistry Materials and Chemical Engineering, Politecnico di Milano, 20133 Milano, Italy*

**K. P. Somers** − *Combustion Chemistry Centre, National University of Ireland Galway, Galway H91 CF50, Ireland*

**Y. Zhang** − *State Key Laboratory of Multiphase Flow in Power Engineering, Xi'an Jiaotong University, Xi'an 710049, China*

**O. Herbinet** − *Laboratoire Réactions et Génie des Procédés, CNRS, Université de Lorraine, ENSIC, 54000 Nancy Cedex, France;* orcid.org/0000-0002-2155-098X

**H. J. Curran** − *Combustion Chemistry Centre, National University of Ireland Galway, Galway H91 CF50, Ireland;* orcid.org/0000-0002-5124-8562

**F. Battin-Leclerc** − *Laboratoire Réactions et Génie des Procédés, CNRS, Université de Lorraine, ENSIC, 54000 Nancy Cedex, France;* orcid.org/0000-0001-8265-7492

**T. Faravelli** − *CRECK Modeling Lab, Department of Chemistry Materials and Chemical Engineering, Politecnico di Milano, 20133 Milano, Italy*

Complete contact information is available at: https://pubs.acs.org/10.1021/acs.energyfuels.0c02252


### Notes

The authors declare no competing financial interest.

## ACKNOWLEDGMENTS

The authors at Politecnico di Milano and CNRS Nancy acknowledge the financial support of IMPROOF project (H2020-IND-CE-2016-17/H2020-SPIRE-S016) within the European Union's Horizon 2020 research and innovation program (grant agreement no. 723706). The authors at NUI Galway wish to acknowledge funding from Science Foundation Ireland (SFI) via project numbers 15/IA/3177 and 16/SP/3829.

## REFERENCES

(1) Pelucchi, M.; Namysl, S.; Ranzi, E.; Rodriguez, A.; Rizzo, C.; Somers, K.; Zhang, Y.; Herbinet, O.; Curran, H.; Battin-Leclerc, F.; Faravelli, T. Combustion of n-C3−C6 linear alcohols: an experimental and kinetic modeling study. Part I: reaction classes, rate rules, model lumping and validation. Submitted to Energy and Fuels, 2020.

(2) Awad, O. I.; Mamat, R.; Ali, O. M.; Sidik, N.; Yusaf, T.; Kadirgama, K.; Kettner, M. Alcohol and ether as alternative fuels in spark ignition engine: A review. *Renewable Sustainable Energy Rev.* **2018**, *82*, 2586−2605.

(3) Kohse-Höinghaus, K.; Oßwald, P.; Cool, T. A.; Kasper, T.; Hansen, N.; Qi, F.; Westbrook, C. K.; Westmoreland, P. R. Biofuel combustion chemistry: from ethanol to biodiesel. *Angew. Chem., Int. Ed.* **2010**, *49*, 3572−3597.

(4) Curran, H. J. Developing detailed chemical kinetic mechanisms for fuel combustion. *Proc. Combust. Inst.* **2019**, *37*, 57−81.

(5) Zhang, K.; Banyon, C.; Bugler, J.; Curran, H. J.; Rodriguez, A.; Herbinet, O.; Battin-Leclerc, F.; B'Chir, C.; Heufer, K. A. An updated experimental and kinetic modeling study of n-heptane oxidation. *Combust. Flame* **2016**, *172*, 116−135.

(6) Brett, L.; MacNamara, J.; Musch, P.; Simmie, J. Simulation of methane autoignition in a rapid compression machine with creviced pistons. *Combust. Flame* **2001**, *124*, 326−329.

(7) Würmel, J.; Simmie, J. CFD studies of a twin-piston rapid compression machine. *Combust. Flame* **2005**, *141*, 417−430.

(8) Morley, C. Gaseq: Chemical equilibria in perfect gases, Version 0.79. 2005, http://www.gaseq.co.uk.

(9) Baigmohammadi, M.; Patel, V.; Martinez, S.; Panigrahy, S.; Ramalingam, A.; Burke, U.; Somers, K. P.; Heufer, K. A.; Pekalski, A.; Curran, H. J. A Comprehensive Experimental and Simulation Study of Ignition Delay Time Characteristics of Single Fuel C1−C2 Hydrocarbons over a Wide Range of Temperatures, Pressures, Equivalence Ratios, and Dilutions. *Energy Fuels* **2020**, *34*, 3755−3771.

(10) Herbinet, O.; Battin-Leclerc, F. Progress in understanding low-temperature organic compound oxidation using a jet-stirred reactor. *Int. J. Chem. Kinet.* **2014**, *46*, 619−639.

(11) Vin, N.; Herbinet, O.; Battin-Leclerc, F. Diethyl ether pyrolysis study in a jet-stirred reactor. *J. Anal. Appl. Pyrolysis* **2016**, *121*, 173−176.

(12) Pelucchi, M.; Namysl, S.; Ranzi, E.; Frassoldati, A.; Herbinet, O.; Battin-Leclerc, F.; Faravelli, T. An experimental and kinetic modelling study of n-C4C6 aldehydes oxidation in a jet-stirred reactor. *Proc. Combust. Inst.* **2019**, *37*, 389−397.

(13) Namysl, S.; Pelucchi, M.; Herbinet, O.; Frassoldati, A.; Faravelli, T.; Battin-Leclerc, F. A first evaluation of butanoic and pentanoic acid oxidation kinetics. *Chem. Eng. J.* **2019**, *373*, 973−984.

(14) Cuoci, A.; Frassoldati, A.; Faravelli, T.; Ranzi, E. OpenSMOKE++: An object-oriented framework for the numerical modeling of reactive systems with detailed kinetic mechanisms. *Comput. Phys. Commun.* **2015**, *192*, 237−264.

(15) Cai, J.; Zhang, L.; Zhang, F.; Wang, Z.; Cheng, Z.; Yuan, W.; Qi, F. Experimental and kinetic modeling study of n-butanol pyrolysis and combustion. *Energy Fuels* **2012**, *26*, 5550−5568.

(16) Li, W.; Zhang, Y.; Mei, B.; Li, Y.; Cao, C.; Zou, J.; Yang, J.; Cheng, Z. Experimental and kinetic modeling study of n-propanol and i-propanol combustion: Flow reactor pyrolysis and laminar flame propagation. *Combust. Flame* **2019**, *207*, 171−185.

(17) Wang, G.; Yuan, W.; Li, Y.; Zhao, L.; Qi, F. Experimental and kinetic modeling study of n-pentanol pyrolysis and combustion. *Combust. Flame* **2015**, *162*, 3277−3287.

(18) Sarathy, S. M.; Oßwald, P.; Hansen, N.; Kohse-Höinghaus, K. Alcohol combustion chemistry. *Prog. Energy Combust. Sci.* **2014**, *44*, 40−102.

(19) Harper, M. R.; Van Geem, K. M.; Pyl, S. P.; Marin, G. B.; Green, W. H. Comprehensive reaction mechanism for n-butanol pyrolysis and combustion. *Combust. Flame* **2011**, *158*, 16−41.

(20) Van de Vijver, R.; Van Geem, K. M.; Marin, G. B.; Zádor, J. Decomposition and isomerization of 1-pentanol radicals and the pyrolysis of 1-pentanol. *Combust. Flame* **2018**, *196*, 500−514.

(21) Sarathy, S. M.; Thomson, M. J.; Togbé, C.; Dagaut, P.; Halter, F.; Mounaim-Rousselle, C. An experimental and kinetic modeling study of n-butanol combustion. *Combust. Flame* **2009**, *156*, 852−864.

(22) Togbe, C.; Dagaut, P.; Mzé-Ahmed, A.; Diévart, P.; Halter, F.; Foucher, F. Experimental and detailed kinetic modeling study of 1-hexanol oxidation in a pressurized jet-stirred reactor and a combustion bomb. *Energy Fuels* **2010**, *24*, 5859−5875.

(23) Togbé, C.; Halter, F.; Foucher, F.; Mounaïm-Rousselle, C.; Dagaut, P. Experimental and detailed kinetic modeling study of 1-

pentanol oxidation in a JSR and combustion in a bomb. *Proc. Combust. Inst.* **2011**, *33*, 367−374.
(24) Power, J.; Somers, K. P.; Zhou, C.-W.; Peukert, S.; Curran, H. J. Theoretical, Experimental, and Modeling Study of the Reaction of Hydrogen Atoms with 1-and 2-Pentene. *J. Phys. Chem. A* **2019**, *123*, 8506−8526.
(25) Sun, Y.; Zhou, C.-W.; Somers, K. P.; Curran, H. J. An Ab Initio/Transition State Theory Study of the Reactions of $\dot{C}5H9$ Species of Relevance to 1, 3-Pentadiene, Part II: Pressure Dependent Rate Constants and Implications for Combustion Modelling. *J. Phys. Chem. A* **2020**, *124*, 4605−4631.
(26) Sun, Y.; Zhou, C.-W.; Somers, K. P.; Curran, H. J. Ab Initio/Transition-State Theory Study of the Reactions of C5H9 Species of Relevance to 1, 3-Pentadiene, Part I: Potential Energy Surfaces, Thermochemistry, and High-Pressure Limiting Rate Constants. *J. Phys. Chem. A* **2019**, *123*, 9019−9052.
(27) Burke, S. M.; Metcalfe, W.; Herbinet, O.; Battin-Leclerc, F.; Haas, F. M.; Santner, J.; Dryer, F. L.; Curran, H. J. An experimental and modeling study of propene oxidation. Part 1: Speciation measurements in jet-stirred and flow reactors. *Combust. Flame* **2014**, *161*, 2765−2784.
(28) Kéromnès, A.; Metcalfe, W. K.; Heufer, K. A.; Donohoe, N.; Das, A. K.; Sung, C.-J.; Herzler, J.; Naumann, C.; Griebel, P.; Mathieu, O.; et al. An experimental and detailed chemical kinetic modeling study of hydrogen and syngas mixture oxidation at elevated pressures. *Combust. Flame* **2013**, *160*, 995−1011.
(29) Metcalfe, W. K.; Burke, S. M.; Ahmed, S. S.; Curran, H. J. A hierarchical and comparative kinetic modeling study of C1− C2 hydrocarbon and oxygenated fuels. *Int. J. Chem. Kinet.* **2013**, *45*, 638−675.
(30) Bagheri, G.; Ranzi, E.; Pelucchi, M.; Parente, A.; Frassoldati, A.; Faravelli, T. Comprehensive kinetic study of combustion technologies for low environmental impact: MILD and OXY-fuel combustion of methane. *Combust. Flame* **2020**, *212*, 142−155.
(31) Ranzi, E.; Cavallotti, C.; Cuoci, A.; Frassoldati, A.; Pelucchi, M.; Faravelli, T. New reaction classes in the kinetic modeling of low temperature oxidation of n-alkanes. *Combust. Flame* **2015**, *162*, 1679−1691.
(32) Dagaut, P.; Sarathy, S.; Thomson, M. A chemical kinetic study of n-butanol oxidation at elevated pressure in a jet stirred reactor. *Proc. Combust. Inst.* **2009**, *32*, 229−237.
(33) Galmiche, B.; Togbe, C.; Dagaut, P.; Halter, F.; Foucher, F. Experimental and detailed kinetic modeling study of the oxidation of 1-propanol in a pressurized jet-stirred reactor (JSR) and a combustion bomb. *Energy Fuels* **2011**, *25*, 2013−2021.
(34) Johnson, M. V.; Goldsborough, S. S.; Serinyel, Z.; O'Toole, P.; Larkin, E.; O'Malley, G.; Curran, H. J. A shock tube study of n-and iso-propanol ignition. *Energy Fuels* **2009**, *23*, 5886−5898.
(35) Stranic, I.; Chase, D. P.; Harmon, J. T.; Yang, S.; Davidson, D. F.; Hanson, R. K. Shock tube measurements of ignition delay times for the butanol isomers. *Combust. Flame* **2012**, *159*, 516−527.
(36) Noorani, K. E.; Akih-Kumgeh, B.; Bergthorson, J. M. Comparative high temperature shock tube ignition of C1− C4 primary alcohols. *Energy Fuels* **2010**, *24*, 5834−5843.
(37) Tang, C.; Wei, L.; Man, X.; Zhang, J.; Huang, Z.; Law, C. K. High temperature ignition delay times of C5 primary alcohols. *Combust. Flame* **2013**, *160*, 520−529.
(38) Heufer, K. A.; Sarathy, S. M.; Curran, H. J.; Davis, A. C.; Westbrook, C. K.; Pitz, W. J. Detailed kinetic modeling study of n-pentanol oxidation. *Energy Fuels* **2012**, *26*, 6678−6685.
(39) Heufer, K.; Bugler, J.; Curran, H. A comparison of longer alkane and alcohol ignition including new experimental results for n-pentanol and n-hexanol. *Proc. Combust. Inst.* **2013**, *34*, 511−518.
(40) Heufer, K.; Fernandes, R.; Olivier, H.; Beeckmann, J.; Röhl, O.; Peters, N. Shock tube investigations of ignition delays of n-butanol at elevated pressures between 770 and 1250 K. *Proc. Combust. Inst.* **2011**, *33*, 359−366.
(41) Black, G.; Curran, H.; Pichon, S.; Simmie, J.; Zhukov, V. Bio-butanol: Combustion properties and detailed chemical kinetic model. *Combust. Flame* **2010**, *157*, 363−373.
(42) Weber, B. W.; Kumar, K.; Zhang, Y.; Sung, C.-J. Autoignition of n-butanol at elevated pressure and low-to-intermediate temperature. *Combust. Flame* **2011**, *158*, 809−819.
(43) Jouzdani, S.; Zhou, A.; Akih-Kumgeh, B. Propanol isomers: Investigation of ignition and pyrolysis time scales. *Combust. Flame* **2017**, *176*, 229−244.
(44) Man, X.; Tang, C.; Zhang, J.; Zhang, Y.; Pan, L.; Huang, Z.; Law, C. K. An experimental and kinetic modeling study of n-propanol and i-propanol ignition at high temperatures. *Combust. Flame* **2014**, *161*, 644−656.
(45) Nativel, D.; Pelucchi, M.; Frassoldati, A.; Comandini, A.; Cuoci, A.; Ranzi, E.; Chaumeix, N.; Faravelli, T. Laminar flame speeds of pentanol isomers: An experimental and modeling study. *Combust. Flame* **2016**, *166*, 1−18.
(46) Ranzi, E.; Frassoldati, A.; Grana, R.; Cuoci, A.; Faravelli, T.; Kelley, A.; Law, C. K. Hierarchical and comparative kinetic modeling of laminar flame speeds of hydrocarbon and oxygenated fuels. *Prog. Energy Combust. Sci.* **2012**, *38*, 468−501.
(47) Davidson, D.; Hanson, R. Interpreting shock tube ignition data. *Int. J. Chem. Kinet.* **2004**, *36*, 510−523.
(48) Vranckx, S.; Heufer, K. A.; Lee, C.; Olivier, H.; Schill, L.; Kopp, W.; Leonhard, K.; Taatjes, C.; Fernandes, R. Role of peroxy chemistry in the high-pressure ignition of n-butanol−Experiments and detailed kinetic modelling. *Combust. Flame* **2011**, *158*, 1444−1455.
(49) Curran, H. J.; Gaffuri, P.; Pitz, W. J.; Westbrook, C. K. A comprehensive modeling study of n-heptane oxidation. *Combust. Flame* **1998**, *114*, 149−177.
(50) Pelucchi, M.; Bissoli, M.; Cavallotti, C.; Cuoci, A.; Faravelli, T.; Frassoldati, A.; Ranzi, E.; Stagni, A. Improved kinetic model of the low-temperature oxidation of n-heptane. *Energy Fuels* **2014**, *28*, 7178−7193.
(51) Ranzi, E.; Gaffuri, P.; Faravelli, T.; Dagaut, P. A wide-range modeling study of n-heptane oxidation. *Combust. Flame* **1995**, *103*, 91−106.
(52) Welz, O.; Klippenstein, S. J.; Harding, L. B.; Taatjes, C. A.; Za'dor, J. Unconventional peroxy chemistry in alcohol oxidation: the water elimination pathway. *J. Phys. Chem. Lett.* **2013**, *4*, 350−354.
(53) Ranzi, E.; Frassoldati, A.; Granata, S.; Faravelli, T. Wide-range kinetic modeling study of the pyrolysis, partial oxidation, and combustion of heavy n-alkanes. *Ind. Eng. Chem. Res.* **2005**, *44*, 5170−5183.
(54) Kerschgens, B.; Cai, L.; Pitsch, H.; Heuser, B.; Pischinger, S. Di-n-buthylether, n-octanol, and n-octane as fuel candidates for diesel engine combustion. *Combust. Flame* **2016**, *163*, 66−78.
(55) Cai, L.; Uygun, Y.; Togbé, C.; Pitsch, H.; Olivier, H.; Dagaut, P.; Sarathy, S. M. An experimental and modeling study of n-octanol combustion. *Proc. Combust. Inst.* **2015**, *35*, 419−427.
(56) Veloo, P. S.; Egolfopoulos, F. N. Studies of n-propanol, iso-propanol, and propane flames. *Combust. Flame* **2011**, *158*, 501−510.
(57) Veloo, P. S.; Wang, Y. L.; Egolfopoulos, F. N.; Westbrook, C. K. A comparative experimental and computational study of methanol, ethanol, and n-butanol flames. *Combust. Flame* **2010**, *157*, 1989−2004.
(58) Katoch, A.; Alfazazi, A.; Sarathy, S. M.; Chauhan, A.; Kumar, R.; Kumar, S. Measurement of laminar burning velocity of n-pentanol+ air mixtures at elevated temperatures and a skeletal kinetic model. *Fuel* **2019**, *237*, 10−17.
(59) Katoch, A.; Chauhan, A.; Kumar, S. Laminar burning velocity of n-propanol and air mixtures at elevated mixture temperatures. *Energy Fuels* **2018**, *32*, 6363−6370.
(60) Beeckmann, J.; Cai, L.; Pitsch, H. Experimental investigation of the laminar burning velocities of methanol, ethanol, n-propanol, and n-butanol at high pressure. *Fuel* **2014**, *117*, 340−350.
(61) Broustail, G.; Halter, F.; Seers, P.; Moréac, G.; Mounaïm-Rousselle, C. Experimental determination of laminar burning velocity for butanol/iso-octane and ethanol/iso-octane blends for different initial pressures. *Fuel* **2013**, *106*, 310−317.
(62) Liu, W.; Kelley, A. P.; Law, C. K. Non-premixed ignition, laminar flame propagation, and mechanism reduction of n-butanol, iso-butanol, and methyl butanoate. *Proc. Combust. Inst.* **2011**, *33*, 995−1002.


https://dx.doi.org/10.1021/acs.energyfuels.0c02252
*Energy Fuels* 2020, 34, 14708−14725

(63) Wang, G.; Li, Y.; Yuan, W.; Wang, Y.; Zhou, Z.; Liu, Y.; Cai, J. Investigation on laminar flame propagation of n-butanol/air and n-butanol/O2/He mixtures at pressures up to 20 atm. *Combust. Flame* **2018**, *191*, 368−380.
(64) Wu, F.; Law, C. K. An experimental and mechanistic study on the laminar flame speed, Markstein length and flame chemistry of the butanol isomers. *Combust. Flame* **2013**, *160*, 2744−2756.
(65) Knorsch, T.; Zackel, A.; Mamaikin, D.; Zigan, L.; Wensing, M. Comparison of different gasoline alternative fuels in terms of laminar burning velocity at increased gas temperatures and exhaust gas recirculation rates. *Energy Fuels* **2014**, *28*, 1446−1452.
(66) Gong, J.; Zhang, S.; Cheng, Y.; Huang, Z.; Tang, C.; Zhang, J. A comparative study of n-propanol, propanal, acetone, and propane combustion in laminar flames. *Proc. Combust. Inst.* **2015**, *35*, 795−801.
(67) Li, Q.; Hu, E.; Zhang, X.; Cheng, Y.; Huang, Z. Laminar flame speeds and flame instabilities of pentanol isomer−air mixtures at elevated temperatures and pressures. *Energy Fuels* **2013**, *27*, 1141−1150.
(68) Li, Q.; Liu, H.; Zhang, Y.; Yan, Z.; Deng, F.; Huang, Z. Experimental and kinetic modeling study of laminar flame characteristics of higher mixed alcohols. *Fuel Process. Technol.* **2019**, *188*, 30−42.


https://dx.doi.org/10.1021/acs.energyfuels.0c02252
*Energy Fuels* 2020, 34, 14708−14725